INVESTIGATION ON MAGNETORESISTORS AS CONTACTLESS CURRENT SENSORS FOR HIGH FREQUENCY POWER ELECTRONIC CONVERTERS

by

Shahriar Jalal Nibir

A thesis submitted to the faculty of
The University of North Carolina at Charlotte
in partial fulfillment of the requirements
for the degree of Master of Science in
Electrical Engineering

Charlotte

2017

Approved by:

_____
Dr. Babak Parkhideh

_____
Dr. Robert Cox

_____
Dr. Badrul Chowdhury

©2017
Shahriar Jalal Nibir
ALL RIGHTS RESERVED

ABSTRACT

SHAHRIAR JALAL NIBIR. Investigation on magnetoresistors as contactless current sensors for high frequency power electronic converters. (Under the direction of DR. BABAK PARKHIDEH)

With the introduction of high frequency semiconductor devices and converters, wideband, lossless and accurate current measurement is the key to achieve highly efficient power conversion. Isolated wideband current measurement is required in many power electronic converters when the switching frequency is above 1 MHz. Typically current passing through a printed circuit board trace induces a highly non-uniform magnetic field which varies as a function of frequency and position relative to the trace. Magnetoresistors (MR) provide an alternative solution to isolated and contactless current monitoring in power converters.

In this work, detailed characterizations of two different Magnetoresistive (MR) elements, the Anisotropic Magnetoresistor (AMR) and the Giant Magnetoresistor (GMR) are performed for contactless current sensing. The AMR and GMR sensor test circuits are designed and implemented in Printed Circuit Boards (PCB) and their performance are evaluated under different spatial and input current conditions including implementation of different sides if the board and DC, AC and step currents up to 10A. Detailed analysis is performed to analyze the sensitivity and sensing range of the sensors. Finally, a frequency analysis is performed on the step current response to evaluate the detection bandwidth of the AMR and GMR current sensors.

Also, this work proposes a technique to increase the frequency bandwidth of Anisotropic Magnetoresistive (AMR) current sensors and simultaneously to intensify and

normalize the field detected by the sensor in the frequency range of interest, i.e., DC-5 MHz. We demonstrate experimentally that the proposed technique yields significant enhancement in detection bandwidth of AMR current sensors.

DEDICATION

To my beloved wife and parents

ACKNOWLEDGMENTS

I would like to take this opportunity to express my great appreciation to my advisor Dr. Babak Parkhideh. He has been very supportive of my work and his thoughtful guidance and feedbacks helped me complete this thesis.

I would also like to thank my committee members, Dr. Robert Cox and Dr. Badrul Chowdhury, for their valuable advice and guidance.

This work has been supported by the National Science Foundation under Award No. 1610250. This work is also supported by Energy Production and Infrastructure Center (EPIC), and Electrical and Computer Engineering Department at University of North Carolina at Charlotte.

I would also like to thank University of North Carolina at Charlotte for Graduate Assistant Support Plan (GASP) award.

Many thanks goes to my fellow students, colleagues and friends at University of North Carolina at Charlotte who have directly or indirectly supported my work.

I would also like to thank my wife Rumana Ferdous Haque for her constant support and also my parents for their support and prayers.

TABLE OF CONTENTS

LIST OF TABLES

LIST OF FIGURES

LIST OF ABBREVIATIONS

AMR	Anisotropic Magnetoresistor
CMR	Colossal Magnetoresistor
CT	Current Transformer
DBC	Direct Bonded Copper
DCR	DC Resistance
EMI	Electromagnetic Interference
FET	Field Effect Transistor
GaN	Gallium Nitride
GMR	Giant Magnetoresistor
IGBT	Insulated Gate Bipolar Transistor
IPEM	Integrated Power Electronic Modules
MOSFET	Metal Oxide Field Effect Transistor
MR	Magnetoresistor
PCB	Printed Circuit Board
SiC	Silicon Carbide
TCR	Resistance Temperature Coefficient
TMR	Tunneling Magnetoresistor
WBG	Wide-Bandgap

CHAPTER 1: INTRODUCTION

1.1 Motivation

Current information is an essential parameter in a wide range of applications in the field of power electronics. Accurate current measurement is a key feature in any power electronic converters and circuits depending on the purposes and requirements such as – control, diagnostics, prognostics and protection. With recent advancement in high frequency power electronics and with the introduction of new generation of wide-bandgap power devices, power electronic converters demand for isolated, lossless, fast and accurate current measurements. Hence, there is a need to investigate alternative approaches and techniques to measure the current in high frequency power converters.

Traditional power electronic converters based on Si switches has their switching frequency limited to a few kilohertz range. On the other hand, the next generation Wide-Bandgap (WBG) switches have the ability to switch at some megahertz. This has enabled the design of faster and miniaturized power converters which are capable of operating at a very high efficiency while maintaining a very small form factor. This significant development in the performance and operation of the power converters has enabled designers to push the boundaries of converters to the next level. However, some new challenges are introduced simultaneously which need to be considered while designing the converters and circuits. At high frequencies, even a small amount parasitic inductance plays a big role in the overall performance and stable operation of the power converter.

These issues, coupled with the higher levels of Electromagnetic Interference (EMI) between the components and traces affects the accuracy of measurement of circuit parameters, especially the current measurements at different locations in the power electronics circuit. Hence, several factors need to be taken into consideration while designing the high frequency converters such as - complex layout considerations, efficient thermal management and effective control algorithms. At the same time, alternative current sensing techniques need to be evaluated for achieving accurate current measurements having isolated, lossless and wideband characteristics.

1.2 Objective of this Study

In the wake of next generation high frequency wide-bandgap power semiconductor switches and the miniaturization of circuits, alternative means for sensing the current information for power electronic converters need to be considered and evaluated. The objective of this study is to investigate alternative current measurement techniques especially, the Magnetoresitor (MR) based current sensing technique for monitoring of currents for high frequency power electronic converters. A detailed literature review on the different approaches to current sensing solutions for power converters is performed. The performance and characteristic of the different current sensing approaches is analyzed for their potential applications in wide-band current sensing. A commercially available Anisotropic Magnetoresistor (AMR) and a Giant Magnetoresitor (GMR) sensor is characterized in terms of DC and AC currents of multiple magnitudes. Finally, a novel wideband current sensing scheme for power electronic converters using the Anisotropic Magnetoresistor (AMR) sensor is proposed.

CHAPTER 2: REVIEW OF CURRENT MEASUREMENT TECHNIQUES FOR POWER ELECTRONIC CONVERTERS

Several current sensing methods for power electronics converters have been investigated by researchers and significant performance improvement have been observed over the years [1]-[6]. In this section, we have compiled a thorough review of different current sensing techniques for power electronic converters from the prospect of implementation and performance. We have divided the most popular current sensing methods two major sections – 1) non-isolated current sensing methods and 2) isolated current sensing methods. Figure 2.1 shows a simple classifications chart of the sensors that are discussed in this literature review section. A brief theoretical background on each current measurement technique is provided and the implementation and performance of the most advanced current sensing technology is discussed in detail. Special focus is given to the implementation of different isolated current sensing methods due to the fact that they are the most advanced sensing technology having the potential to be implemented in next generation Wide-Bandgap power converters as well as Integrated Power Electronic Modules (IPEM). Section 2.1 discusses the non-isolated current sensing techniques such as sense resistor, inductor internal resistance and SenseFET. Section 2.3 summarizes the most advanced and popular isolated current sensing methods such as – Current transformer, Rogowski coil, Hall-effect sensor, Magnetoresistor sensor and Hybrid sensors. Finally, in Section 2.5, an overall evaluation of all the current sensing techniques in terms of application, performance and implementation is provided and the

conclusion is drawn highlighting the most effective solutions for current sensing for next generation power electronics converters.

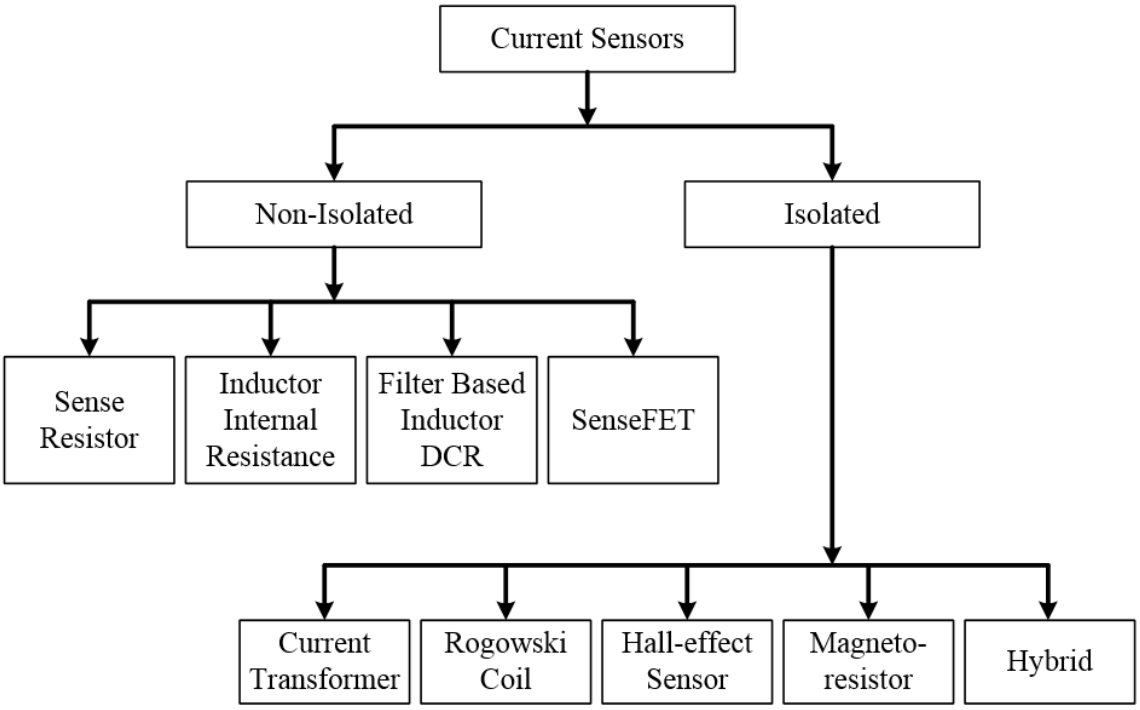

Figure 2.1: Classification of different current sensing methods

2.1 Non-Isolated Current Sensing Methods

2.1.1 Current Sense Resistor

Current sensing based on the sense resistor is the simplest method to measure the current in a power electronic converter. A high precision sense resistor is placed in series with the current path in consideration and the voltage drop across the resistor is a simple representation of the actual current. Sense resistors usually have a very low resistance and temperature coefficient of resistance. Figure 2.2 shows the implementation of a sense

resistor to measure the inductor current of a buck converter. Current measurement through sense resistors follow Ohm's law and the voltage across the resistor is,

$$V_{sense} = i_L * R_{sesnse}$$

Since the value of the sense resistor is precisely known, the actual current through the inductor and the sense resistor is directly proportional to the measured voltage across the resistor. Usually they are implemented with Kelvin connections for improved accuracy.

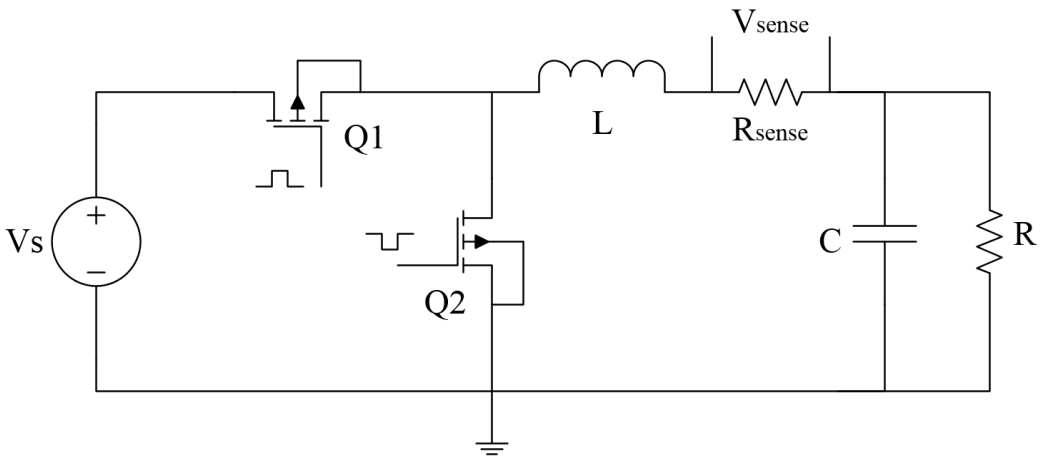

Figure 2.2: Current measurement based on sense resistor

The sense resistor is suitable for both AC and DC current measurement but does not provide any galvanic isolation which makes them unsuitable for certain applications. Some researchers have discussed a few isolation techniques is [7]-[9] but they add to the cost and complexity in implementation of the techniques. Besides, the sense resistor is added directly on to the main current path which causes power loss. Also, the parasitic inductance of the sense resistor at high switching frequencies introduces noise in the

current measurement and additional circuits are required to filter out the noises. The sense resistor based current sensing techniques can be implemented for low frequency, high current applications as well as high frequency, low current applications. For high frequency, high current applications, the resistor value has to be significantly lower to keep the power losses at a minimum level which makes it extremely difficult to retrieve the ripple current information with good accuracy. The factors that need to be considered while selecting a sense resistor for current measurement in high frequency power electronic converters are - accuracy, inductance, efficiency, power loss and cost.

2.1.2 Internal Resistance of Inductor

External sense resistors introduces unnecessary power loss and loss of efficiency in power converters. To avoid the issues associated with and external sense resistor, the internal resistor of the main inductor of a power converter can be utilized to extract the current information [10]. The voltage across the inductor (L) having an internal resistance (RL) is measured to be,

$$V = L\frac{di_L}{dt} + i_L R_L$$

If a second inductor is coupled with the first one having the same number of turns then the first component of equation (2) can be measured on the secondary windings. Subtracting this quantity from the main inductor voltage gives the voltage which is directly proportional to the current in the inductor. Figure 2.3 shows the current sensing scheme utilizing the internal resistance of an inductor.

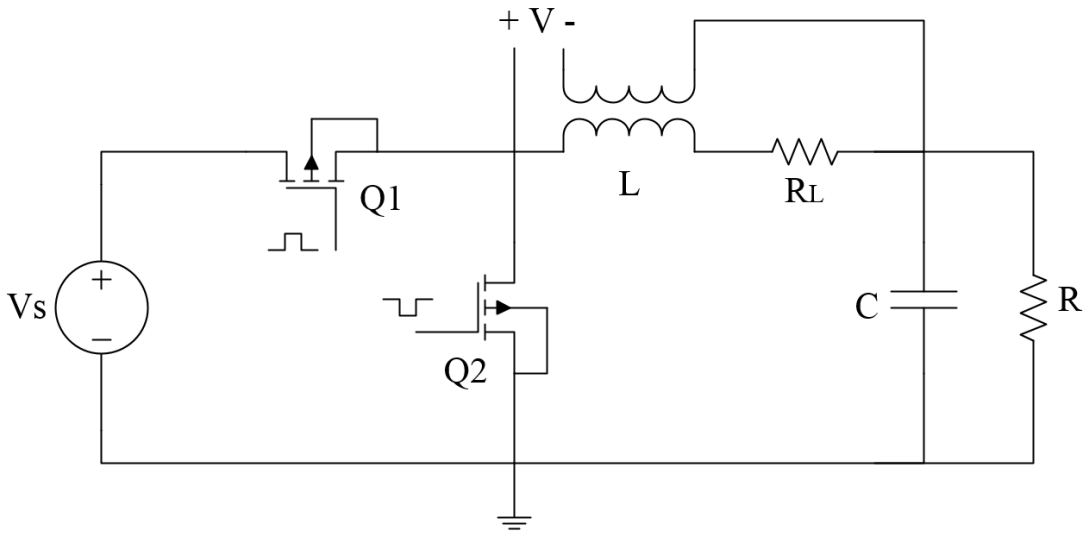

Figure 2.3: Current sensing based on internal resistance of inductor

This method has the advantage of lower cost and higher efficiency in power converter as no external resistor needs to be implemented. This is appropriate for low frequency, high current applications. However, this method can be implemented only for obtaining the inductor current information which varies based on the topology of the converter. Hence, in many applications this method cannot be utilized for measuring switch currents as well as currents in the desired section. Also the calibration and the temperature coefficient of the inductor resistance need to be considered for high accuracy measurement.

2.1.3 Filter Based Inductor DCR Current Sensing

The internal resistance of the inductor can be utilized in another way to achieve lossless current measurement in power electronic converters. The internal DC Resistance (DCR) of an inductor has a very low tolerance which makes it a very attractive solution

for measuring currents in high efficiency power converters. A RC filter network is added in parallel to the inductor (L) with internal resistance (RL). Figure 2.4 shows the implementation of the RC filter network across the inductor in order to extract the indictor current information.

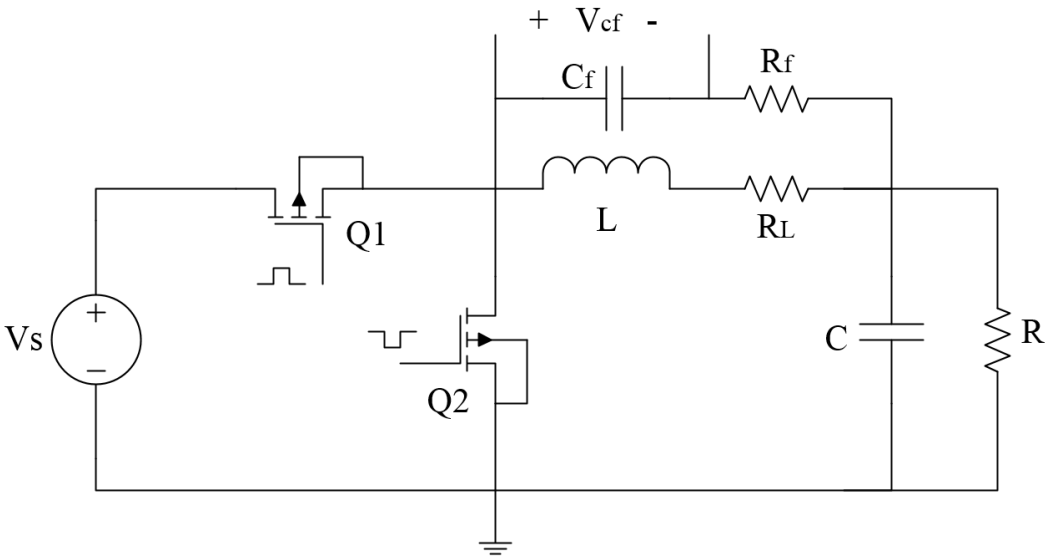

Figure 2.4: Filter based inductor DCR current sensing

The voltage across the filter capacitor Cf is,

$$V_{C_f} = \left(\frac{Ls + R_L}{R_f C_f s + 1}\right) i_L$$

The equation can be rearranged as,

$$V_{C_f} = \left(\frac{\frac{L}{R_L}s + 1}{R_f C_f s + 1}\right) i_L R_L$$

If the filter Rf and Cf values are selected in such a way that,

$$R_f C_f = \frac{L}{R_L}$$

Then, the voltage across the capacitor is,

$$V_{C_f} = i_L R_L$$

Hence, the inductor current becomes directly proportional to the measured capacitor voltage.

One of the biggest challenges of implementing this method is the time constant mismatch. If the time constant of the filter (RfCf) does not equal the (L/RL) ratio, then the measured current waveform is distorted because of the change in slew rate of charging and discharging of the inductor. The issue is discussed in [11]-[12] and some design considerations are suggested to mitigate the problem. In [13] the design and analysis of the DCR sensing method for low tolerance and high accuracy current measurements are discussed. The DCR current sensing method can be implemented in a power electronic converter for lossless and accurate current measurements as well as effective current-mode control algorithms as demonstrated by [14]-[16].

The DCR current sensing method is lossless and has very high accuracy. Other advantages of this method are high bandwidth, low sensing noise, low cost and low volume. However, this method does not provide any galvanic isolation and only the inductor current can be measured with this method. This technique cannot be applied to measure the switch current information or current in other desired sections of a power electronic converter.

2.1.4 SenseFET

Current sensing with SenseFET technique originally came from current mirroring in MOSFET integrated in electronic circuits. In most of the fabrication FET transistors

either in lateral or vertical, thousands of individual cells are interconnected in parallel configurations. Ideally, since these cell arrays are all identical, by isolating the source connection of one or several cells, a new pin can be considered for sensing that monitors proportionally the active switch current [17].

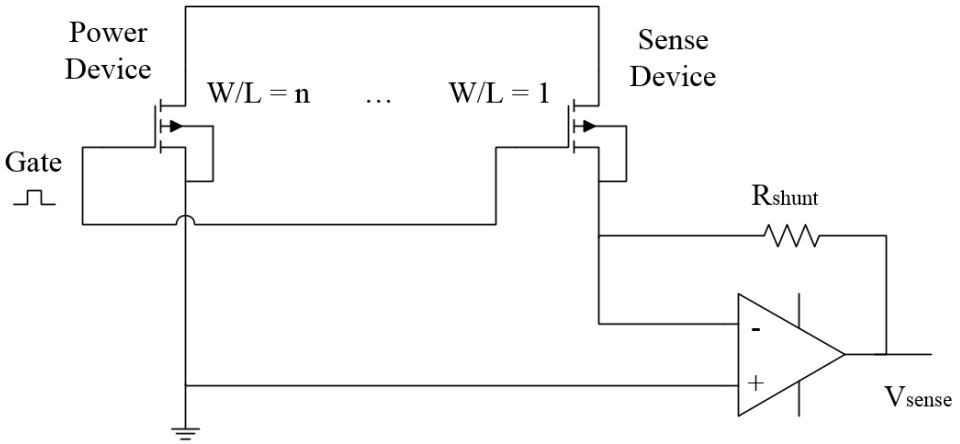

Figure 2.5: Current sensing based on SenseFET

Since the sensing transistor has the common drain and gate with the power transistor, by neglecting the small fraction of voltage drop across the sensing resistor, the gate-source signal can be assumed the same for both power and sense FET. Furthermore, the amplifier circuits force the same drain-source voltage drop across the power transistor. Therefore, it is expected that the voltage drop across the sensing resistor proportionally shows the drain-source current of the main power transistor. This also provides an opportunity to change the length-width ratio channel of the FET, which directly reflects on the transistor turn-on resistance. The scaled down version of the main current stream of the drain can pass through the transistor with smaller W/L ratio and would dramatically improve the loss compared to other resistive techniques like shunt

resistor measurement. In the integrated switch, the combination of parallel cells can be arranged as power and SenseFET. Figure 2.5 shows a typical sensing scheme using a SenseFET.

Theoretically, this technique does not suffer any bandwidth limitations and can be perceived as very high accurate measurement technique; however, in practice the voltage sampling and current measurement accuracy might be varied due to the temperature dependency of FET ON-resistance, sensing resistor, and mismatching of gate-source signals. Moreover, for WBG semiconductors such as GaN, the drain-source resistor during on-time, increases at higher voltages like MOSFETs, which also needs to be considered. To mitigate the effect of temperature dependency, and current ratio mismatching of sensing transistor, it is required to optimize sensing resistor based on the proposed technology. To compensate the effect of impedance matching, virtual grounding for tightly holding the common source for both transistors (power and sensing transistor) should be carefully designed. Furthermore, some recommendations such as choosing higher resistance on turn-on path of sensing resistor to provide proper delay and reducing spikes during transients [18], designing high gain amplifier to improve the accuracy [19] as well as some practical guidelines for integrated SenseFET [20] should be taken into an account.

Recently, this approach has been demonstrated for SiC and GaN devices integrated with Si MOSFET [21]-[22]. Figure 2.6(a) shows the prototype demonstrated in [21] with SiC on Si approach and Figure 2.6(b) shows the prototype demonstrated in [22] with GaN on Si approach. SiC MOSFET with integrated current sense with SiC transistor is demonstrated in [23] as shown in Figure 2.6(c). SenseFET is typically non-isolated and

hence, applicable for grounded devices where the common-mode voltage is higher than 30V. This approach can be cost-effective if all integrated into the device die, and have been commercially used for some monitoring and protection purposes [24]-[27]. Figure 2.6 shows the prototype for current mirroring technique implemented using GaN switches.

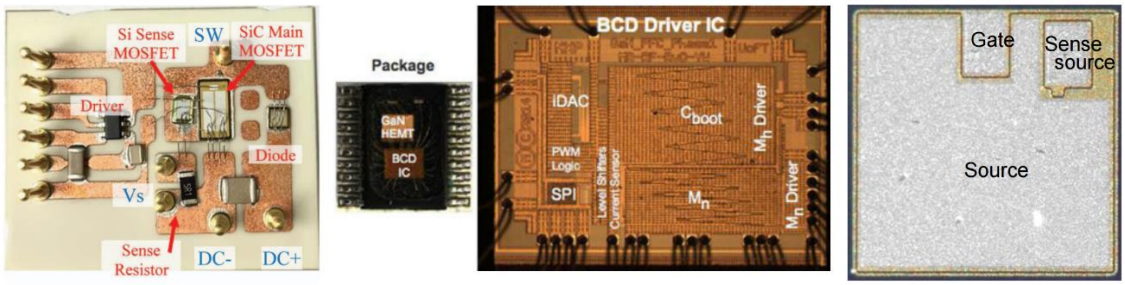

(a) (b) (c)

Figure 2.6: Different approaches for current sensing using SenseFET technology (a) SiC on Si approach [21], (b) GaN on Si approach [22], (c) SiC on SiC approach [23]

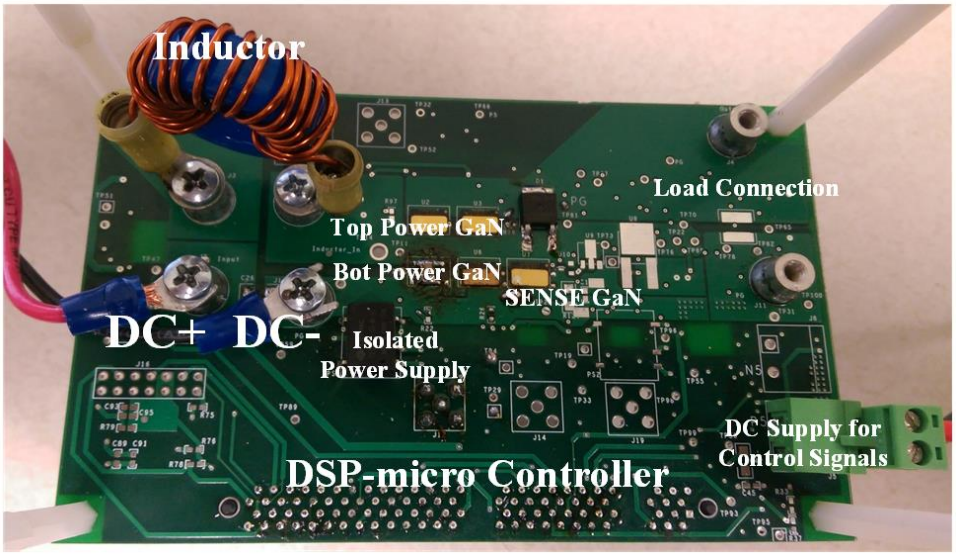

Figure 2.6: Prototype for current mirroring technique implemented using GaN switches

2.2 Isolated Current Sensing Methods

2.2.1 Current Transformer

Currents Transformers (CT) are widely used for AC current measurements in different applications. The CT has the advantage of galvanic isolation and low power consumption. This method introduces the current in the secondary winding of a transformer and potentially has high performance for current measurement. Although previously these transformers have been built in bulky, nowadays some companies like Coilcraft released high performance current transformer sensor in small packages which are able to measure the current at 20A, 48V and 1MHz [28]-[29].

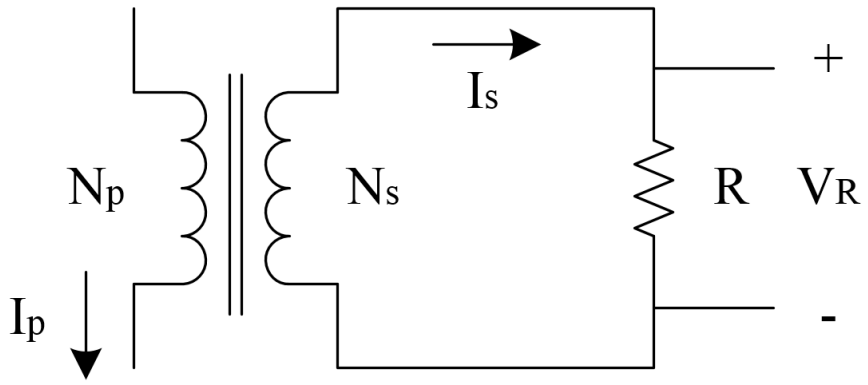

Figure 2.7: Current sensing based on current transformer

The basic operating schematic of a CT is shown in Figure 2.7. A CT typically has a single turn primary and a multi turn secondary winding. The primary and secondary sides are wound around a laminated magnetic core made with ferromagnetic materials.

The current is passed through the primary winding of the CT which induces a current in the secondary following the faradays induction principal. The secondary side of the CT is terminated in to a resistor. The voltage across the resistor is measured which corresponds to the secondary side current. Based on the turn ratio of the CT, the primary current information is extracted. Typically, too many turns in the secondary side is avoided due to the fact that it introduces unnecessary inter-winding capacitance.

If the turn ratio of the CT is Np/Ns, then the relationship between the primary current (Ip) and the secondary current (Is) in the CT can be expressed as,

$$\frac{N_p}{N_s} = \frac{I_s}{I_p}$$

If the secondary winding is terminated in resistor R, then the voltage across the resistor (VR) is,

$$V_R = I_s R$$

Combining the above two equations,

$$V_R = \frac{N_p}{N_s} I_p R$$

Hence, the primary current becomes directly proportional to the measured voltage across the secondary terminating resistance.

In DC current transformer, they typically have at least two cores with a rectifier, then the voltage drop across a resistor at the measurement section can provide current information [30]. DC current measurement has also been realized by using CT in conjunction with RL multi-vibrator [31]. Due to the utilization of coil inductors, they can suffer from the saturation at high switching frequency, and their typical applications in the market are not going beyond 100 kHz. The CT can also be used to measure the

inductor current of a power converter and is being widely used by several researchers in different power electronic applications [32]-[39].

The CT can enable lossless, isolated and accurate current measurement for power electronic converters. However, the magnetic core used for the coupling between the primary and secondary side of the transformer suffers from saturation due to its use of ferromagnetic materials. Besides, for higher current ratings, the secondary windings has to be increased significantly as well as the core size. Typically, the size of the current transformer is quite big. Moreover, the primary side is in line with the main current path which increases the inductance in the current path. That's why the application of the CT is not ideal in some topologies.

2.2.2 Rogowski Coil

A Rogowski coil is a magnetic coupling transducer that delivers an output signal which is ideally proportional to the time derivative of the input current. Rogowski coil based current sensing, due to its inherent simplicity, and no bandwidth limitation is among the most popular techniques in high frequency power converters. The Rogowski coil based current sensor typically consists of an air-core inductor coil with a few number of turns, which is placed around the main current carrying conductor. The air core Rogowski coil is induced by current of the main conductor. Then the picked up current information is transformed to equivalent voltage through an integrator circuit. In some applications, the coil is equipped with a periodic reset signal to indicate the start and end point for integration. The Rogowski coil is a simple, lossless and accurate current sensing

method for detecting currents and is investigated and implemented in several applications over the years [40]-[48].

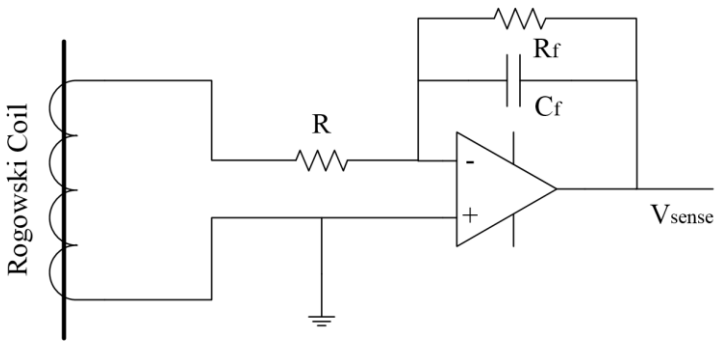

Figure 2.8: Current sensing based on Rogowski coil

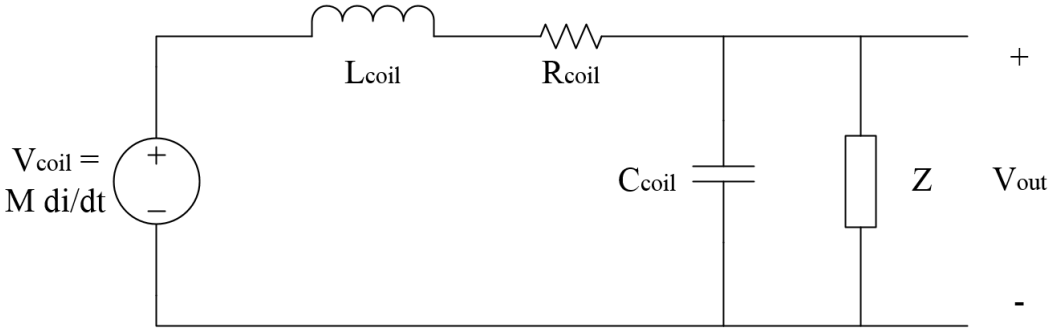

Figure 2.9: Equivalent circuit of a Rogowski coil

Figure 2.8 shows the schematic diagram of a typical Rogowski coil. The coil responds to the transient current in the main conductor path and generates an output signal which is proportional to the time derivative of the current. The coil output voltage Vcoil is,

$$V_{coil} = M\frac{di}{dt}$$

An integration of the coil output voltage is required to extract the actual current information. However, in practice, there are non-idealities such as leakage inductance and inter-winding capacitance that need to be considered in the design.

Figure 2.9 shows the equivalent circuit of a Rogowski coil taking into account the non-ideal quantities. In this circuit, Rcoil is the coil resistance, Lcoil is the coil leakage inductance and Ccoil is the aggregated inter-winding capacitance. Z is the terminating impedance of the Rogowski coil. The transfer function of the Rogowski coil can be obtained from the equivalent circuit as,

$$\frac{V_{out}}{I_{in}} = \frac{ZMs}{ZL_{coil}C_{coil}s^2 + (L_{coil} + ZR_{coil}C_{coil})s + (R_{coil} + Z)}$$

$$\approx \frac{Ms}{L_{coil}C_{coil}s^2 + R_{coil}C_{coil}s + 1}\Big|_{Z\to\infty}$$

Assuming high impedance output for the Rogowski coil, one should design the coil such that 1) sufficient mutual inductance to maintain the required sensitivity at particular frequency range is obtained, and 2) the natural frequency of the resonance as seen in (4) is located far enough from the required sensor bandwidth.

The Rogowski coil generates an output which is the time derivative of the current. Hence, this method of measuring current responds to only AC transients and is not applicable for DC currents. The Rogowski coil requires an integrator in the coil output to get the actual current information. An active integrator allows to adjust the gain with slower response to faster rise times while a passive integrator allows for faster rise time response with a lower gain. The main difficulty with implementing the Rogowski coil is optimizing the design for low and high frequency operations as discussed in [41]. The

problem is rectified using active RC integration for low frequency bands and passive RC integration for higher frequency bands [41].

The Rogowski coil has been implemented in an integrated chip. Silicon Labs has developed a Rogowski coil based single chip AC current sensor (Si85XX) for measurements up to 20A [49]. The sensor adds on 2nH inductance in the current path while providing low loss isolated current measurements with and accuracy of +/-5%. Figure 2.10 shows the functional block diagram of the Rogowski coil sensor. The sensor requires the integrator capacitor to be discharged at the beginning of each measurement cycle which is achieved by an external reset signal synchronized with the gate signals of the converter switches.

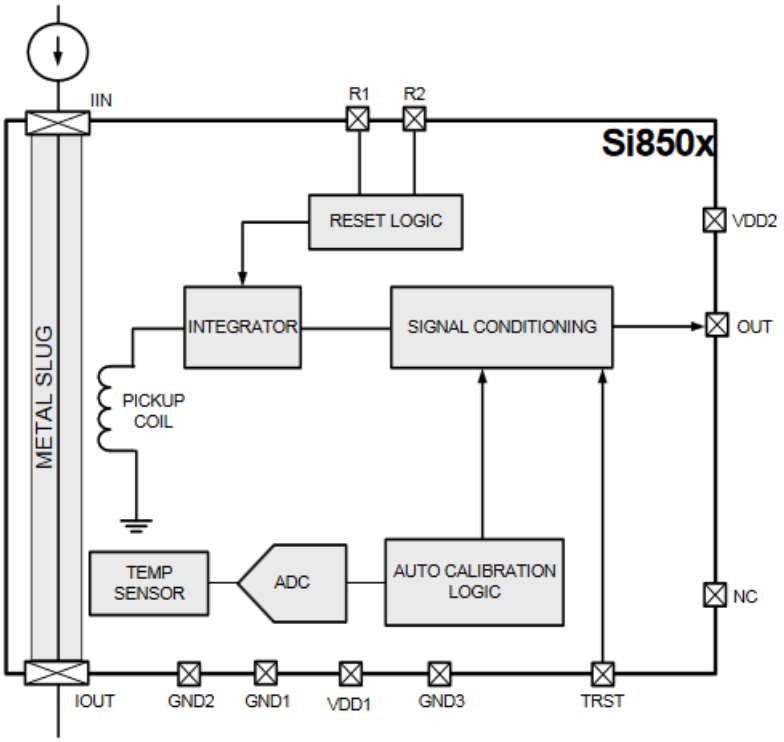

Figure 2.10: Functional block diagram of the Si85XX Rogowski coil current sensor [49]

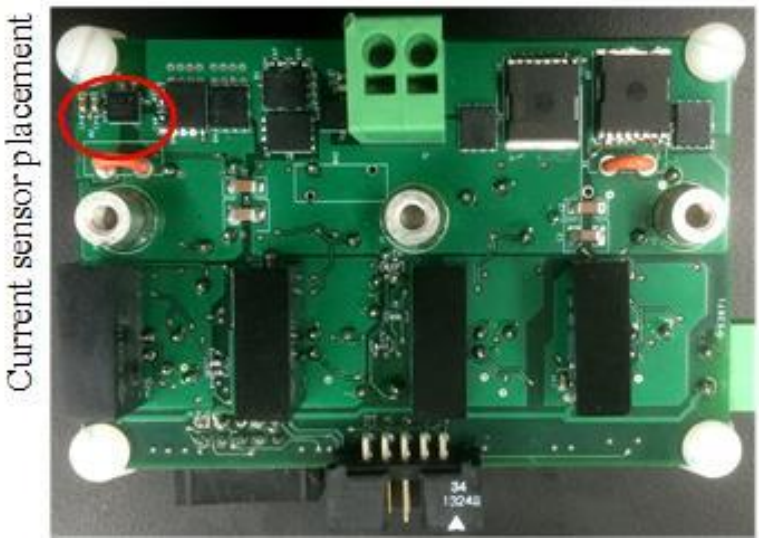

Figure 2.11: Rogowski coil current sensor (Si85XX) implemented in a 500 kHz PV inverter for switch current measurement

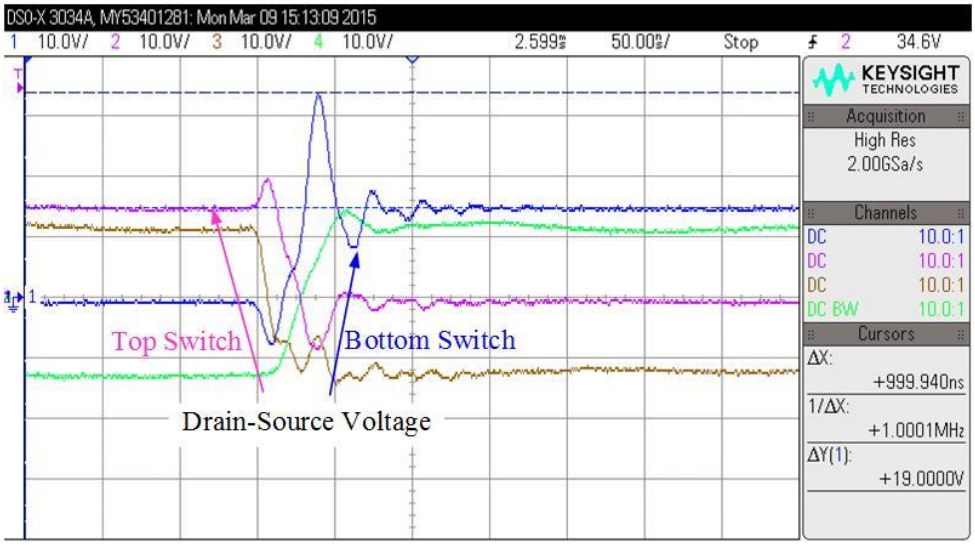

Figure 2.12: Overshoot in the switch voltages observed in the 500 kHz PV inverter

The Rogowski coil sensors developed by Silicon Labs are used in a 500 kHz PV inverter for measuring the two switch currents for control and diagnostic purposes. Figure 2.11 shows the developed prototype of the 500 kHz PV inverter equipped with the Rogowski coil sensors. The performance of this design is carefully studied and we

concluded that the addition of a few nano-henry of inductance due to the trace interruption and insertion of the current sensor leads to have a significant overshoot voltage seen by the switches. As can be seen in Figure 2.12, there is a 19V overshoot voltage on a 15V bus voltage seen by the switch. Hence, the Rogowski coil sensor on chip requires a lot of layout considerations and introduces complexities in the converter design and implementation.

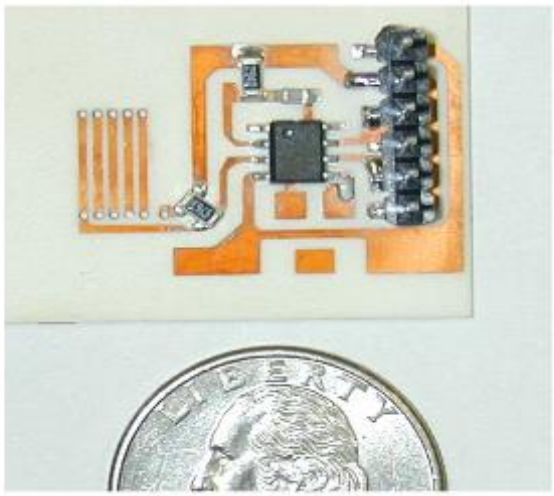

Figure 2.13: Planar embedded Rogowski coil developed for IPEMs [52]

The Rogowski coil can also be implemented on a Printed Circuit Board (PCB). PCB Rogowski coils has the advantage of lower size, lower parasitic capacitance, high accuracy, low tolerance and wide bandwidth. The PCB planar Rogowski coil has been successfully implemented for very high di/dt current measurements [50]-[51]. A compact planar embedded Rogowski coil design is proposed in [52] for Integrated Power Electronic Modules (IPEM) with high linearity and wide operation bandwidth. Figure 2.13(a) shows the prototype for the planar embedded Rogowski coil developed in [52].

The coil embedded in between two bus conductors and can be implemented on both 4 layer and 2 layer PCB depending on the configuration. It has been claimed that, the proposed structure in [52] has excellent linearity with frequency, temperature and current magnitude as well as low cost and promising integration possibility.

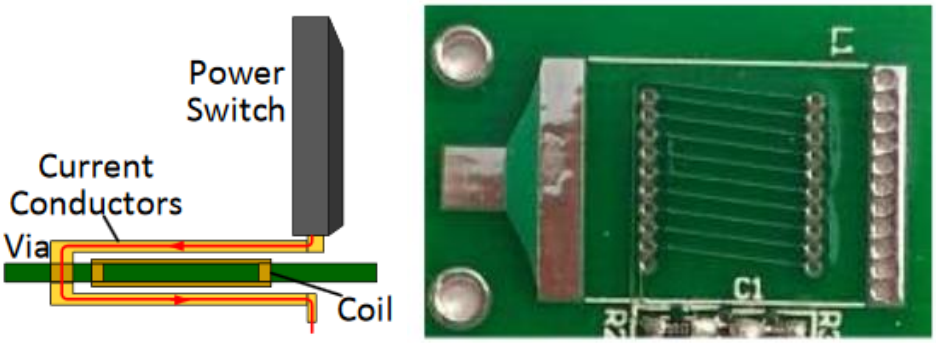

Figure 2.14: PCB embedded Rogowski coil [53]

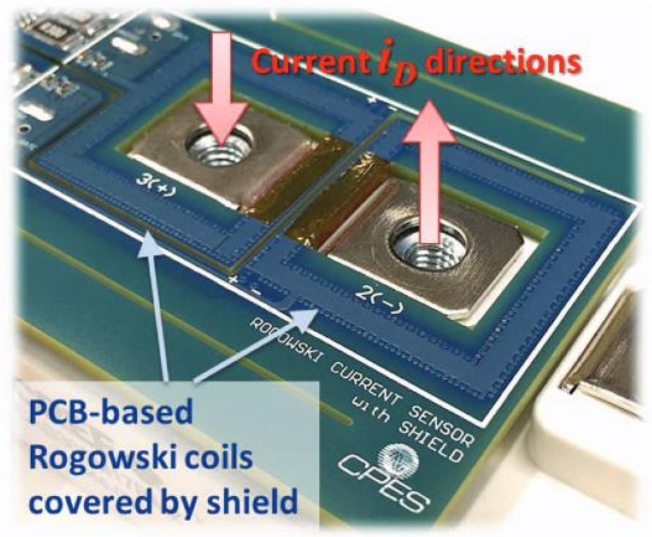

Figure 2.15: Shield covered PCB embedded Rogowski coil [55]

Another example of the PCB embedded Rogowski coil implementation is demonstrated in [53]. In [53], the Rogowski coil is realized in a 2 layer PCB with claimed simulation sensing bandwidth between 2.66Hz and 100MHz with a sensitivity of 0.0715A/V. Figure 2.14 shows the prototype PCB embedded Rogowski coil developed in [53]. The PCB embedded Rogowski coil method of sensing currents are also implemented in several medium to high voltage power electronic converters using Wide-Bandgap (WBG) semiconductor (SiC) switches and various aspects are discussed in [54]-[55]. Figure 2.15 shows the shield covered PCB embedded Rogowski coil developed in [55].

2.2.3 Hall-Effect Based Current Sensing

Today, Hall-effect devices make up by far the largest part of all magnetic sensors in the market. They are used in a broad range of applications. Hall-effect is a galvano-magnetic effect occurring in a piece of conductor or semiconductor biased by electrical current and exposed to magnetic field. Enforced by Lorentz law, if the biased element is exposed to a magnetic field (normal component) the trajectory of carriers is deflected. The voltage across the element changes due to the deflection of charge carriers and it can be measured and interpreted as the magnetic field strength. Due to the required normal component of the magnetic field for the Hall element to react, the device is sandwiched in the airgap of a magnetic core wrapping around the current carrying wire as shown in the setup in Figure 2.16.

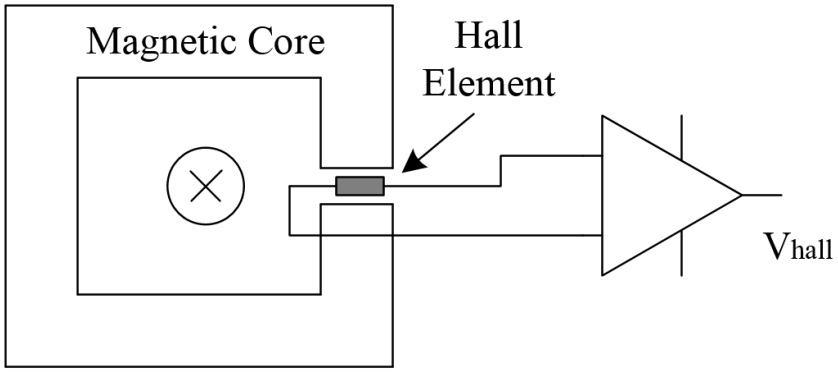

Figure 2.16: Current sensing based on Hall-effect sensors

Typical Si-based integrated Hall sensors have their bandwidth is limited to a few tens of kilohertz. Using materials with higher carrier mobility than Si such as GaAs and InAs allows to reduce the thickness of the element while the element becomes more sensitive and can pick up faster transients of the magnetic field. Very recently, an integrated 20A Hall current sensor (CQ3303), from AKM Japan, using thin-layer InAs was introduced with 1MHz bandwidth and operating temperature range from -40◦C to +80◦C [56]. InAs has low bandgap of 0.36 eV compared to Si, 1.10eV, and is prone to temperature drift; however, by proper characterizations of the element, temperature compensation circuits can be designed. The design of these circuits can be much more challenging using materials such as InSb that has much higher mobility but with very low band gap of 0.18 eV. Figure 2.17 shows the functional block diagram of the InAs based Hall-effect based current sensor from AKM. Allegro Microsystems has also recently released a Hall-effect based current sensor IC (ACS730) having 1 MHz bandwidth and 210 ns response time [57]. Both the CQ3303 and ACS 730 are capable of isolated current sensing but it requires the main conductor path to pass through the sensor IC for local

field generation and sensing. This requires some layout modifications and design considerations for minimizing effect on the other aspects of the high frequency power converter.

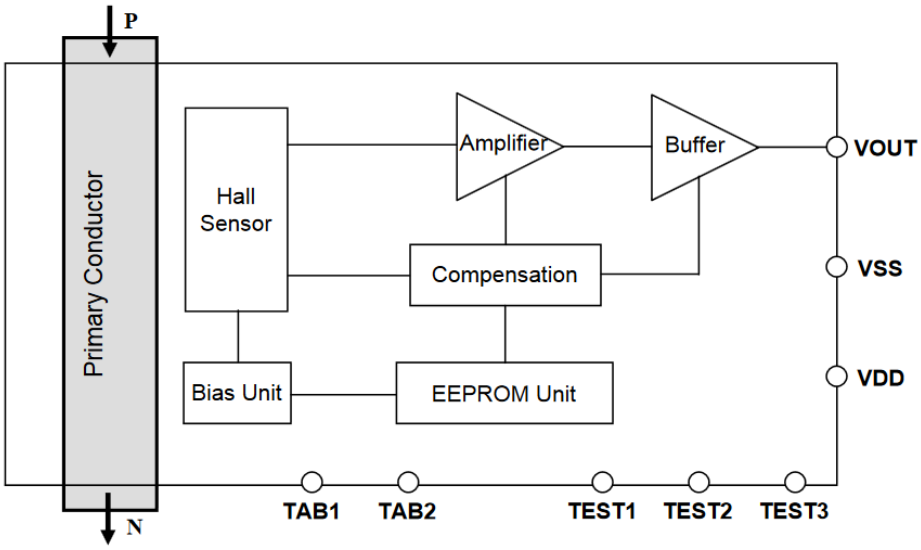

Figure 2.17: Functional block diagram of the current sensor developed by AKM [56]

Hall-effect sensors can detect both AC and DC fields making then suitable for many power electronic applications. The Hall elements can be fabricated in a chip using conventional CMOS process. Several research groups are investigating on the Hall-effect sensors and significant development has been observed over the years [58]-[63]. The integrated versions of the Hall-effect current sensor, mostly open-loop, is much more attractive for volume cautious designers. Using these integrated solutions requires a change in the layout of the circuit or switch bonding and is not suitable for many high frequency designs.

Conventional planar Hall technology is only sensitive to the flux density applied orthogonally to the IC's surface. Pioneered by Prof. Popovic's research group at EPFL, Switzerland, a contact-less hall sensor was proposed [64]-[65] in which parallel field produced by the current in a wire or a PCB trace is picked up by two carefully designed ferromagnetic plates separated by a defined air gap. These two plates function as a magnetic concentrator that pulls in the field. The proposed concentrator converts locally the parallel field with the chip surface into a field perpendicular to the chip surface right at the edge of the air gap. Placing the Hall element right underneath the air gap edge allows the element to react to the magnetic field and hence the producing current information can be deduced. Figure 2.18 shows Popovic's method of implementing magnetic concentrators for Hall devices. The concept has been commercialized by Melexis and the bandwidth goes up to 250 kHz [66]. The sensor developed by Melexis offers fully isolated contactless solution to DC and AC current measurements for up to 250 kHz.

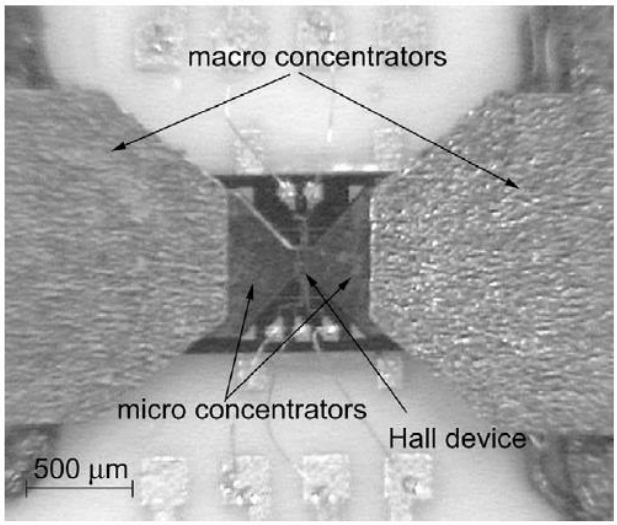

Figure 2.18: Implementation of magnetic concentrators on Hall devices [65]

2.2.4 Magnetoresistor (MR) Based Current Sensing

Magnetoresistors are the simplest of Lorentz force devices, using semiconductors such as InSb and InAs. The magnetoresistive sensors can be fabricated both from semiconductors and metal alloys, which permits the conductivity and the sensitivity to be tailored precisely to the application. In contrast to Hall-effect sensors, magnetoresistive sensors do not suffer from drift and are less susceptible to external noise, increasing their attraction for application in high frequency power electronics. The increased flexibility in design has led to the evolution of five different types of magnetoresistive elements in the search for a magnetic reading and storage technology: the Magneto-Resistor (MR), the Anisotropic Magneto-Resistor (AMR), the Giant Magneto-Resistor (GMR), the Colossal Magneto-Resistor (CMR), and the Tunneling Magneto-Resistor (TMR). The difference between different types of magnetoresistive elements lies predominantly in their sensitivity to the magnetic field and the linearity of their response. Whereas MRs and AMRs display a more linear response and little to no hysteresis compared to GMRs, CMRs, and TMRs, they are also less sensitive. The increased sensitivity to magnetic field of GMRs, CMRs, and TMRs comes with several disadvantages, including higher instability with change in temperature (high TCR), higher resistance, and hysteresis. The Anisotropic Magnetoresistor (AMR) and Giant Magnetoresistor (GMR) are two of the most popular MR technologies used in current sensing applications.

MR sensors are generally capable of responding to very high frequency fields due to the inherent property of the magnetoresistive elements. MR sensors, like Hall-effect sensors, can detect both AC and DC fields which makes them very useful in current sensing for power electronic converters. In contrast to Hall-effect sensors, the MR

sensors respond to the horizontal components of the magnetic field. The typical implementation of a MR based current sensor is shown in Figure 2.19.

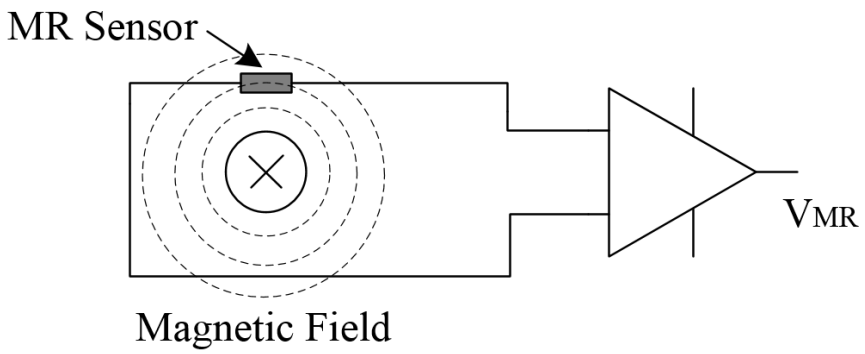

Figure 2.19: Current sensing based on Magnetoresistor sensors

Anisotropic Magnetoresistors (AMR) show a change in their resistivity when exposed to an external magnetic field. AMRs are based on metal alloys as shown in Figure 2.20. The most widely used AMR device developed and integrated into a chip is composed of four Permalloy (Ni0.81Fe0.19) AMRs in a full sensitivity Wheatstone bridge configuration. In the AMR element shown in Figure 2.20, M and biased I are shown in their default directions when no magnetic field is applied. M is aligned with the easy axis, and I is directed along the shortest distance between the conducting strips like Aluminum. The natural zero energy orientation state of the material is defined as the easy axis, and a relatively small applied magnetic field will reach the saturation magnetization of the material along this direction. In contrast, along the hard axis a substantially larger magnetic field is necessary to reach the saturation magnetization.

The direction of current flow in a material is controlled by the location of the contacts across which a voltage is applied. If the material is designed such that contacts

are at an angle to the easy axis, and initially when no field is present the magnetization is oriented along the easy axis, the conduction path is the shortest distance between the contacts. By applying a magnetic field in the plane defined by the easy axis and the distance between the electrical contacts, which is perpendicular to easy axis, the magnetization is rotated from the easy axis towards the direction of current flow, in effect changing the orientation of dipoles, increasing the current path. This increase in current path translates into an increase in resistance in the material as a function of the applied magnetic field.

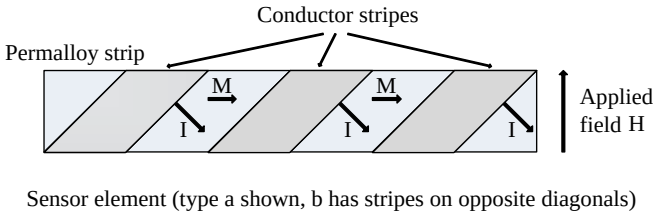

Figure 2.20: An example of AMR element. M (magnetization) and I (bias) are shown in their default directions when no magnetic field is applied

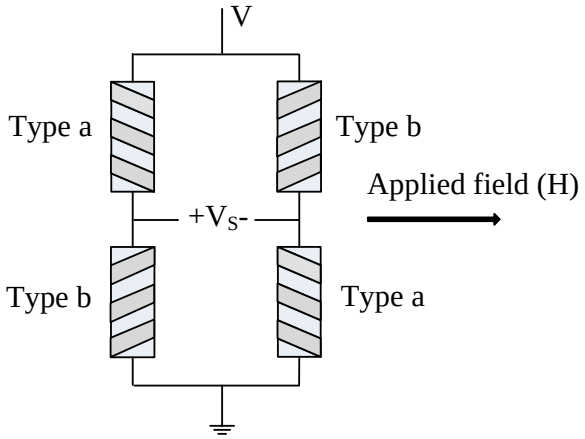

Figure 2.21: AMR elements in a Wheatstone bridge configuration

When the magnetization is aligned with the direction of current flow, defined by the location of the contacts, the resistance reaches its maximum value. In the type of

AMR shown in Figure 2.20 (known as type ‘a’), the applied field forces the angle between M and I to increase, decreasing the resistance. If the conducting strips are placed along opposite diagonals (mirror-imaged along the vertical axis), the applied field reduces the angle between M and I, increasing the resistance. This arrangement is known as type ‘b’. By combining both types of AMR elements in a Wheatstone bridge as shown in Figure 2.21, such that one output produces the sum of the resistances induced by the magnetic, and the other so that the resistances compensate for each other, the output can be further amplified.

When the AMR elements arranged in the Wheatstone bridge configuration are exposed to an external magnetic field, the subsequent change in resistance of the elements results in a voltage differential in the bridge output. The resistance changes linearly with the magnetic field and so does the bridge output. Hence, a linear change in the bridge output is observed which is proportional to the change in the magnetic field. This property of the AMR element is utilized to detect the magnetic field generated by the current in a conductor and consequently tuned as a current sensor.

The AMR sensors can respond to magnetics fields generated by very high frequency currents. In a typical power electronic application, the MR-based current sensor is placed on top or underneath a PCB trace carrying the current without any conductive contact to the trace. Figure 2.22(a) shows the standard configuration of a MR based current sensor for detecting current. The most advanced commercially available contactless AMR sensor developed by Honeywell [67] has a theoretical detection bandwidth of 5 MHz. However, at high frequency currents, especially above 1 MHz, the current tends to flow through the edges of the trace due to skin effect. The magnetic field

due to high frequency currents is visualized in Figure 2.22 (b). Hence, the sensor detects the weaker part of the field and loses its performance. However, normalizing the magnetic fields over the frequency range of interest by means of magnetic concentrators as simple as the folded trace technique demonstrated in [68] results in a much higher detection bandwidth from the sensor. Investigation on the AMR sensor positioning and effective layout recommendations for peak current control of a 30V, 3A synchronous buck converter running at 1 MHz switching frequency is presented in [69].

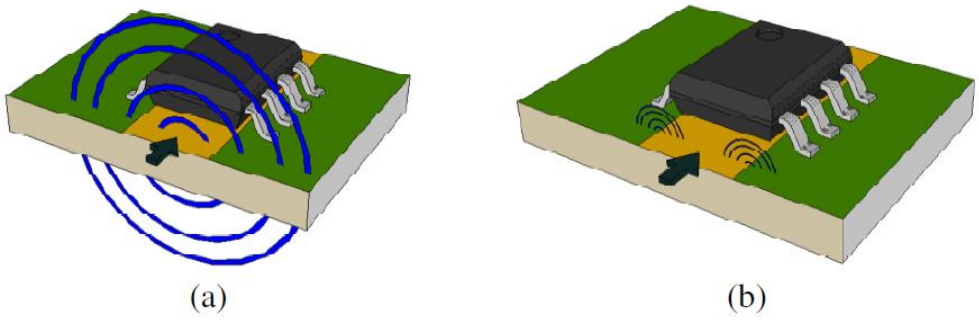

Figure 2.22: (a) Magnetic field distribution at low frequencies, (b) Magnetic field distribution at high frequencies due to skin effect

Sensitec has also developed a dynamic current sensor (CMS 3000 series) based on the AMR elements with a sensing bandwidth of up to 2 MHz [70]-[71]. Figure 2.23 shows the functional diagram of the sensor developed by Sensitec Gmbh for current sensing up to 2 MHz. However, these sensors are relatively larger in size and require the current to pass through the sensor which leads to change in the layout for a power electronic converter. The AMR based current sensors developed by Sensitec are utilized for current measurement in a boost converter running at 1 MHz demonstrated in [72]. Several practical applications of the Sensitec AMR based current sensors are demonstrated in [73]-[75].

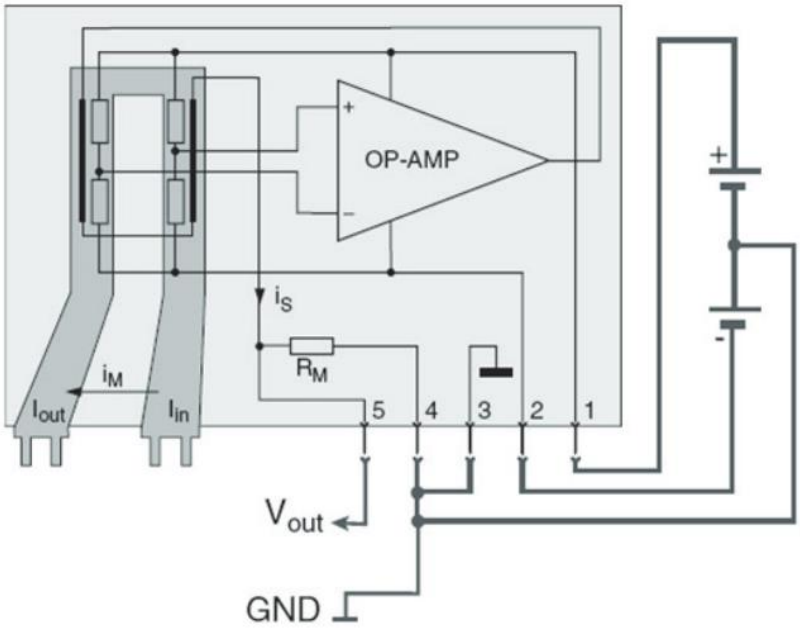

Figure 2.23: Functional diagram of the current sensor developed by Sensitec

The Giant Magnetoresistive effect is found in metallic thin films that consists of extremely thin magnetic layers separated by equally thing nonmagnetic layers. When an external magnetic field is applied, the resistance of the material is reduced significantly. Very weak changes in the magnetic resistance of the element results in big differences in the electrical resistance. At room temperature, GMRs show a change in resistance of up to 12.8% due to magnetic fields compared to 2%–4% for the AMR [76]. The best utilization of GMR materials as point field detectors is in a Wheatstone bridge formation as shown in Figure 2.24. Small magnetic shields are placed on top of two GMR resistors on the opposite sides of the Wheatstone bridge. These shields allows the resistors to act as reference resistors as the applied magnetic fields have no effect on them. The remaining two GMR resistors are exposed to the applied magnetic field and in presence

of an external magnetic field their electrical resistance decreases which generates a voltage in the bridge output. Additional flux concentrators are sometimes used to adjust the sensitivity of the bridge. The output of the Wheatstone bridge is proportional to the applied magnetic field and biased at half the provided supply voltage.

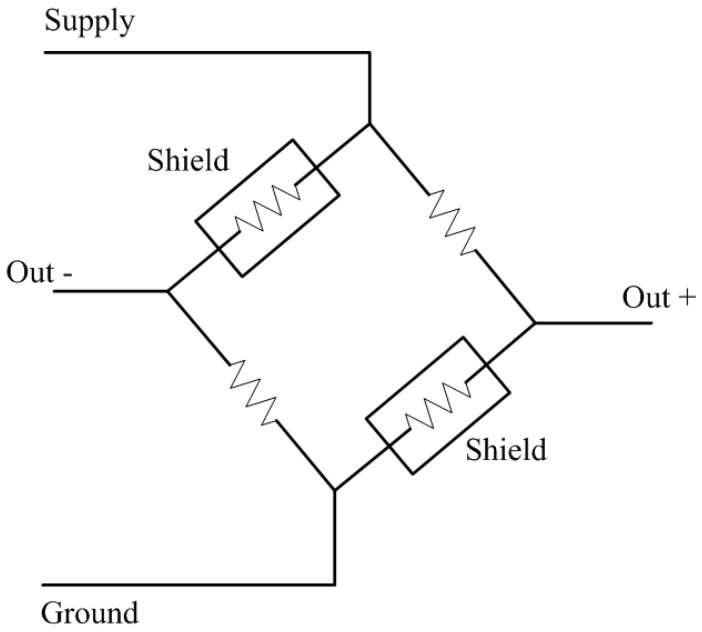

Figure 2.24: GMR point field detectors in Wheatstone bridge configuration

GMR sensors can respond to much weaker magnetic fields when compared to AMR sensors. That's why GMR sensors can provide improved sensitivity and much better sensing resolution than the AMR sensors [77]. However, the GMR sensors suffer from hysteresis which negatively affects the performance of the sensors in detecting currents [78]. Researchers are investigating in to the hysteresis issues and several methods are proposed to linearize the GMR sensor output based on effective hysteresis modelling and hysteresis compensation [79]-[83].

Due to the huge potential of GMR sensors for high frequency current sensing in power electronic converters, researchers are focusing on the integration possibility of GMR sensors into power modules. Figure 2.25 shows the implementation of the GMR current sensors on flex circuit integrated in a planar power module consisting of Direct Bonded Copper (DBC) IGBTs [84]-[85].

Figure 2.25: GMR current sensors implemented for measuring currents in IGBTs [84]

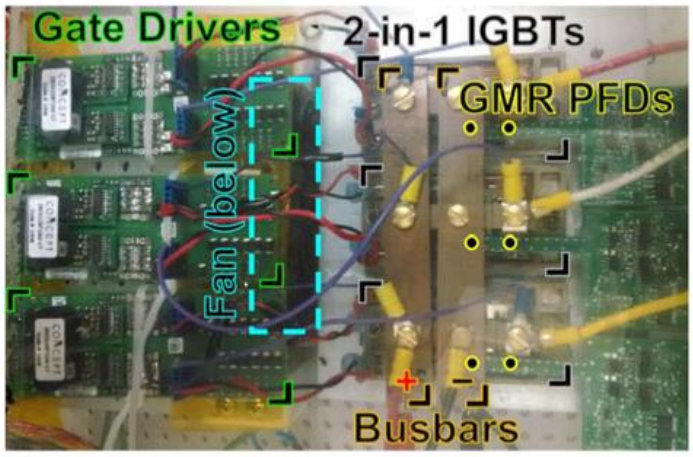

Figure 2.26: GMR sensors for current measurement and control of a 3 phase inverter [86]

Prof. Lorenz's research group from University of Wisconsin-Madison has conducted detailed investigation in the integration of GMR sensors into power modules

[86]-[92]. Figure 2.26 shows Lorenz's implementation of GMR sensors for current measurement and control of a 3 phase inverter. The GMR sensor integrated into power modules has also been suggested for thermal measurement in [88]. The GMR sensor is also successfully implemented and verified in a low voltage high current voltage regulator module for 1V and 15A running at 1 MHz switching frequency [93]-[94]. Also, some other applications of GMR is demonstrated in different applications showing the potential for isolated and contactless current measurement in power electronic converters [95]-[97].

2.2.5 Hybrid Sensor

Hybrid current sensors combine multiple current sensing technologies together to achieve a superior performance and accurate measurement. Usually, two different sensing technologies are selected for two different frequency range of operation to achieve an extreme wideband performance characteristics. The low frequency sensor is responsible for detecting transients from DC to a certain frequency. The high frequency sensor is active after the low frequency sensor limit and extends to a much higher operation frequency. Several post processing circuits are required to condition and combine the output of the low frequency and high frequency sensors to achieve a wideband response.

Some of the popular choices for the low frequency current measurement of the hybrid sensors are Hall-effect sensors and Magnetoresitor (MR) based sensors whereas, for the high frequency measurements, Current Transformers (CT) and Rogowski coil are the most popular solutions for its low cost and very high frequency response characteristics. Several researches are investigating in the hybrid current sensors to

improve the performance, bandwidth, linearity and accuracy of current sensing [98]-[107].

The concept of hybrid current sensors were first reported in [98]-[99] using a Hall-effect based sensor for detecting low frequency currents and a PCB Rogowski coil for high frequency current sensing. The sensor developed in [98]-[99], also known as the HOKA probe is claimed to be able to respond to high frequency transients of up to 50 MHz. The developed prototype has been experimentally tested for DC current measurements up to 200A and high di/dt transients of up to 2.5kA/us with only +/-5% full scale error [98]. The design also eliminates the requirement for integrating the Rogowski coil output as the Rogowski coil is utilized for measuring the high frequency transients only. The HOKA probe performance is further analyzed with a planar PCB air-coil sensor in multi-chip IGBT modules [100].

Prof. Kolar's research group based in ETH Zurich, Switzerland has demonstrated a hybrid sensor utilizing Hall-effect sensor and current transformer for current measurements of up to +/-50A and bandwidth of 20 MHz [101]. The concept is further developed and a planar version of the hybrid sensor utilizing Hall-effect sensor and current transformer is proposed in [102]-[103] with a measurement bandwidth from DC to 30 MHz and current ratings of 40A. The Hall-effect sensor is positioned in the airgap of the magnetic structure while the current transformer is realized in a planar structure with multilayer PCB winding. Figure 2.27 shows the hybrid sensor prototype developed in [102]-[103]. The hybrid sensor is claimed to have excellent linearity and high dv/dt immunity.

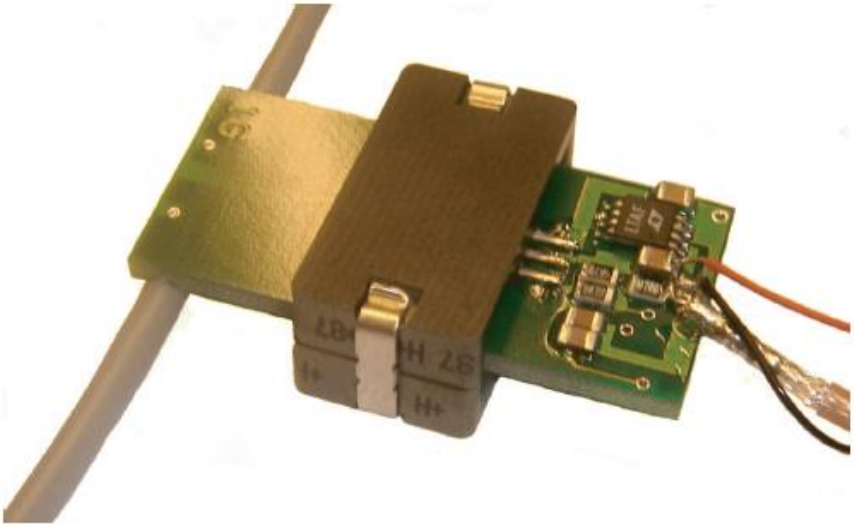

Figure 2.27: Hybrid current sensor comprising of Hall-effect sensor and current transformer developed in [102]-[103]

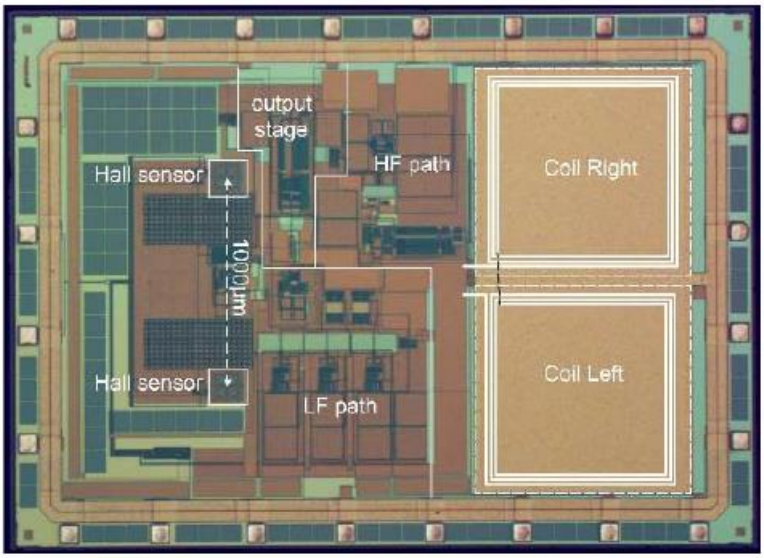

Figure 2.28: Integrated hybrid multipath current sensor comprising of Hall-effect sensor and Rogowski coil developed in [104]-[105]

Researchers in Delft University of Technology in Netherlands have proposed an integrated wideband hybrid sensor based on Hall-effect sensors and Rogowski coil [104]-[105]. The sensor is fabricated using 0.18um standard CMOS process and the claimed

sensing bandwidth is 3 MHz. Figure 2.28 shows the developed sensor chip in [104]-[105] using 0.18um standard CMOS process. The sensor has been experimentally tested to measure step currents of up to 3A magnitude.

MR based sensors also show good potential to be used as low frequency current detectors in hybrid sensor configurations. A hybrid current sensing scheme utilizing an AMR sensor and the low frequency sensor and a planar Rogowski coil sensor as the high frequency sensor is demonstrated in [106]-[107]. The hybrid sensor takes advantage of the proposed magnetic field concentrators using conductive materials for normalizing the magnetic field generated by the current for high bandwidth current measurements from DC to 10 MHz. The sensor has been experimentally tested for current measurements up to 10A.

2.3 Conclusion

In this chapter, a detailed review on different current sensing techniques has been performed. The current sensing methods are evaluated in terms of two major approaches – non-isolated and isolated. Several non-isolated current measurement methods staring from the simplest sense resistor to the state of the art SenseFET are discussed in detail from both theoretical and implementation point of view. The limitations associated with these sensing methods, such as the time constant mismatch issue for filter based inductor DCR current sensing and temperature dependency of the SenseFET, are analyzed and different solutions proposed in many recent articles are discussed. Specially, the implementation of SenseFET utilizing the most advanced wide-bandgap semiconductor based transistors are analyzed for high frequency current sensing solutions.

The isolated current sensing methods offer loss-less and accurate current measurement solutions and are more suitable for high frequency applications. In this chapter, several isolated current sensing techniques such as – current transformer, Rogowski coil, Hall-effect and magnetoresistors are discussed in detail. Current transformers can offer very accurate current measurements but their big size and difficulty in detecting DC currents make them unsuitable for high frequency converters applications. Rogowski coil has an air core hence, does not suffer from saturation. Besides, the flexibility in design offered by Rogowski coil in the form of planar and PCB embedded coils makes them an excellent choice for high frequency power electronic applications and integrated current sensing solutions. Hall-effect and magnetoresistors are both excellent candidates for isolated and lossless current sensing in power electronic converters. Magnetoresitive sensors has the advantage of responding to horizontal magnetic fields compared to the Hall-effect sensors which respond to the vertical components of the magnetic field. The sensing bandwidth of the MR sensors are much higher than the Hall-effect sensors which makes it an ideal candidate for applications such as high frequency power converters. The summary of different isolated current sensing techniques are presented in Table 2.1.

Table 2.1: Summary of different isolated current measurement techniques

	CT Transformer	Rogowski Coil (Integrated)	Hall-effect	AMR	GMR
Bandwidth	10 kHz – 1 MHz	50 kHz – 1 MHz	DC – 1 MHz	DC – 5 MHz	DC – > 1 MHz
Sensitivity	-	400 mV/A	60 mV/A	10 mV/V/mT	20-32 mV/V/mT
Rating	20 A	20 A	20 A	0.6 mT	1.4 mT
Error	-	5%	1.3%	1.6%	2%
Temperature	–40°C to +125°C	–40°C to +125°C	–40°C to +125°C	–55°C to +150°C	–50°C to +125°C

CHAPTER 3: CHARACTERIZATION OF MAGNETORESISTORS FOR CONTACTLESS CURRENT SENSING FOR POWER ELECTRONIC APPLICATIONS

Extraction of the current information in high frequency converters is one of the major challenges in high frequency power electronics. With the introduction of state of the art wide-bandgap (WBG) power devices, the operating frequency of the power electronic converters is pushing into the MHz domain which results in significant reduction in the size of the passive components and circuits. The switching noise generated by the power semiconductor devices in conjunction with the Electromagnetic Interference (EMI) between the different components of the circuit, have an extremely adverse effect on the performance of the converter specially on the switch current and inductor current information which are the most essential parameters for effective control of the power electronic converters. Traditional current sensing techniques such as resistor-based, filter based and inductor based techniques are not suitable for measurement of currents in high frequency converters. Alternative current measurement techniques such as series MOSFET's on-resistance and parallel current-sensing FET (SenseFET) don't provide electrical isolation. Hence, isolated, contactless, high bandwidth and accurate current measurements techniques are required for high frequency (>1 MHz) power electronic converters using high voltage (>30V) wide-bandgap devices.

Hall-effect based sensors, Magnetoresistors (MR) based sensors and Rogowski coils are some of the most popular solutions for isolated and contactless current sensing.

Rogowski coils respond to only AC transients and are not capable of detecting the DC currents for power electronic converters. Hall-effect sensors are widely used in different applications as they can respond to both AC and DC fields but limited by a bandwidth of a few kHz. Hence, they are unsuitable for high frequency (>1 MHz) contactless current measurement.

Magnetoresistor (MR) sensors are developed based on metal alloys compared to hall-effect sensors which are made from silicon. MR sensors have excellent sensitivity and measurement accuracy as they suffer from less drift and are less immune to noise. They can respond to both AC and DC fields and has a very high detection bandwidth which makes them an attractive choice for high frequency current sensing in power electronic converters. The increased flexibility in design has led to the evolution of five different types of magnetoresistive elements: the magnetoresistor (MR), the anisotropic magnetoresistor (AMR), the giant magnetoresistor (GMR), the colossal magneto-resistor (CMR), and the tunneling magneto-resistor (TMR). The difference between different types of magnetoresistive elements lies predominantly in their sensitivity to the magnetic field and the linearity of their response. Whereas MRs and AMRs display a more linear response and little to no hysteresis compared to GMRs, CMRs, and TMRs, they are also less sensitive. Several research groups are investigating on techniques to improve the sensitivity and accuracy of current sensing by MR and GMR devices for power electronics applications.

In this chapter, we have evaluated the performance of two different magnetoresistive elements - AMR and GMR in terms of measuring currents in power electronic converters. Two different commercially available sensors are selected based on

their sensitivity and detection range. Test circuits are developed using the sensors for contactless measurement of current and the circuits are implemented in a 4 layer Printed Circuit Board (PCB). The sensor performances are analyzed for measuring DC, AC and step currents running through a PCB trace having different distances from the sensing element. The results are analyzed and a frequency response is performed to analyze the detection bandwidth of the AMR and GMR sensor.

3.1 Magnetoresistor (MR) Technologies for Current Sensing

The Anisotropic Magnetoresistor (AMR) and Giant Magnetoresistor (GMR) are two of the most popular MR technologies used in current sensing applications. A brief discussion about these technologies are presented in the following section.

3.1.1 Anisotropic Magnetoresistor (AMR)

Anisotropic Magnetoresistors show a change in their resistivity when exposed to an external magnetic field. The most widely used AMR device developed and integrated into a chip is composed of four Permalloy (Ni0.81Fe0.19) AMRs in a full sensitivity Wheatstone bridge configuration [67]. In the AMR element shown in Figure 3.1, M and biased I are shown in their default directions when no magnetic field is applied. In the type of AMR shown in Figure 3.1 (known as type ‘a’), the applied field forces the angle between M and I to increase, decreasing the resistance. If the conducting strips are placed along opposite diagonals (mirror-imaged along the vertical axis), the applied field reduces the angle between M and I, increasing the resistance. This arrangement is known

as type ‘b’. By combining both types of AMR elements in a Wheatstone bridge as shown in Figure 3.2, such that one output produces the sum of the resistances induced by the magnetic, and the other so that the resistances compensate for each other, the output can be further amplified.

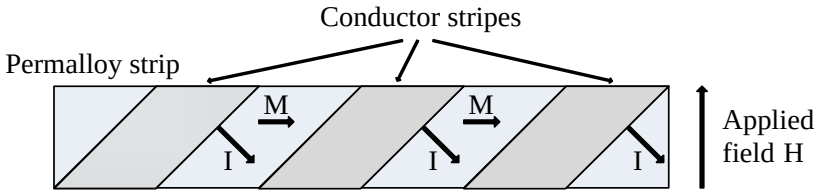

Sensor element (type a shown, b has stripes on opposite diagonals)

Figure 3.1: An example of AMR element. M (magnetization) and I (bias) are shown in their default directions when no magnetic field is applied

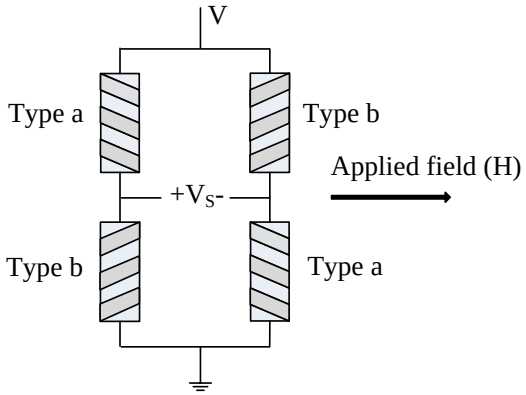

Figure 3.2: AMR elements in a Wheatstone bridge configuration

3.1.2 Giant Magnetoresistor (GMR)

The Giant Magnetoresistive effect is found in metallic thin films that consists of extremely thin magnetic layers separated by equally thing nonmagnetic layers. When an

external magnetic field is applied, the resistance of the material is reduced significantly. Very weak changes in the magnetic resistance of the element results in big differences in the electrical resistance [77]. The best utilization of GMR materials as point field detectors is in a Wheatstone bridge formation as shown in Figure 3.3. Small magnetic shields are placed on top of two GMR resistors on the opposite sides of the Wheatstone bridge. These shields allows the resistors to act as reference resistors as the applied magnetic fields have no effect on them. The remaining two GMR resistors are exposed to the applied magnetic field and in presence of an external magnetic field their electrical resistance decreases which generates a voltage in the bridge output. Additional flux concentrators are sometimes used to adjust the sensitivity of the bridge. The output of the Wheatstone bridge is proportional to the applied magnetic field and biased at half the provided supply voltage.

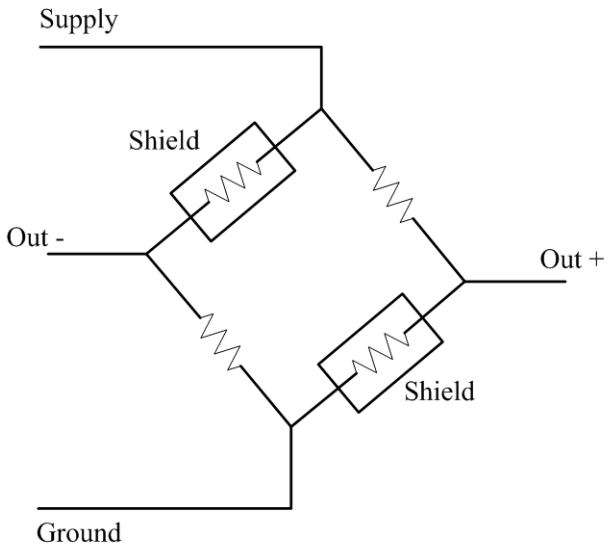

Figure 3.3: GMR point field detectors in Wheatstone bridge configuration

3.2 Experimental Results and Discussion

To characterize the magnetoresistive sensors in terms of current measurement, two commercially available AMR and GMR sensors are selected based on the sensitivity and sensing range. For AMR sensor, Honeywell HMC1021S is selected. The HMC1021S is a single axis surface mount sensors for detection of low magnitude magnetic fields [67]. The magnetoresistive sensors are made of a Permalloy thin-film deposited on a silicon wafer [67]. When and external magnetic field is applied, the bridge resistive elements are changed which corresponds to a change in the bridge output voltage. The sensor has two on-chip magnetically coupled straps, the offset strap and the set/reset strap for incident field and magnetic domain alignment.

For GMR sensor, NVE Corporation AA003-02 is selected. This sensor is also single axis and the output is unipolar in nature which means that the magnetic field applied along the sensitive axis will generate the same output for positive and negative direction of magnetic field [77]. The output is also proportional to the supply voltage and is biased at half the supply voltage. Some basic specifications of the selected AMR (Honeywell HMC1021S) and GMR (NVE Corporation AA003-02) sensors are presented in Table 3.1.

Table 3.1. Specifications for Honeywell HMC1021S and NVE Corporation AA003-02 Magnetoresistors

Sensor Type	Model	Sensing Range		Sensitivity (mV/V/mT)	Bandwidth (MHz)	Hysteresis (%)	Operating Temperature (^{0}C)
		Min. (mT)	Max. (mT)				
AMR	HMC1021S	-0.6	0.6	10	5	0.08	-55 to 150
GMR	AA003-02	0.2	1.4	20 – 32	> 1	4	-50 to 125

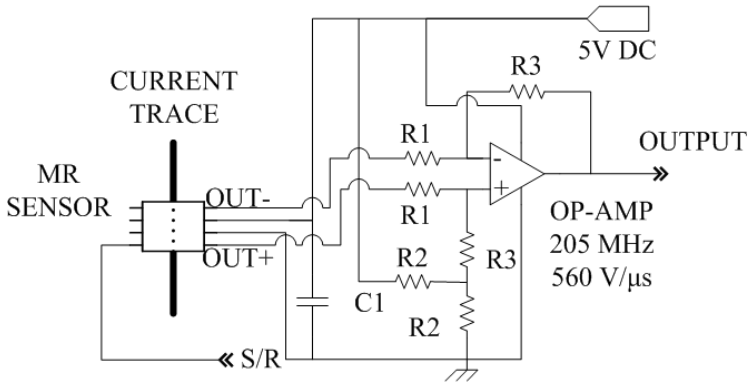

Figure 3.4: Circuit diagram of the hardware setup for evaluation of magnetoresitor based current sensors

To evaluate the performance of the sensors as current monitoring devices, several circuits were developed. The circuit diagram of the hardware setup developed for the experiment are presented in Figure 3.4. The output of the sensor was amplified using a differential amplifier circuit using a high bandwidth and high slew rate operational amplifier. The bridge output voltage from the GMR sensor is higher than the AMR sensor due to the inherent property of GMR. Hence, the GMR experimental setup was developed with a differential gain of 7.7 whereas the GMR setup was developed with a differential gain of 20.

The designed circuit was implemented on a 4 layer PCB using 1 Oz copper. Four different prototypes of the sensors were developed with two each for AMR and GMR sensors running current traces at different distances from the sensor. On one prototype test board for each sensor, the sensor and the current trace were placed on the same side (top layer) of the PCB which translates to a distance of 0.75mm between the current trance and the sensing element. On the other prototypes, the sensor and the current trace were placed on opposite side of the PCB which translates to a distance of 2.32mm

between the current trace and the sensing element. The developed prototypes are shown in Figure 3.5 and Figure 3.6.

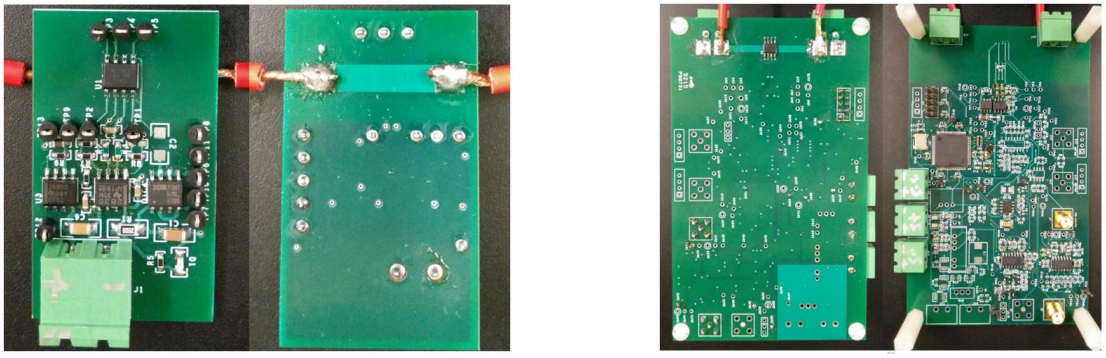

(a) (b)

Figure 3.5: AMR evaluation board with distance between sensor and the current trace (a) 2.32mm and (b) 0.75mm

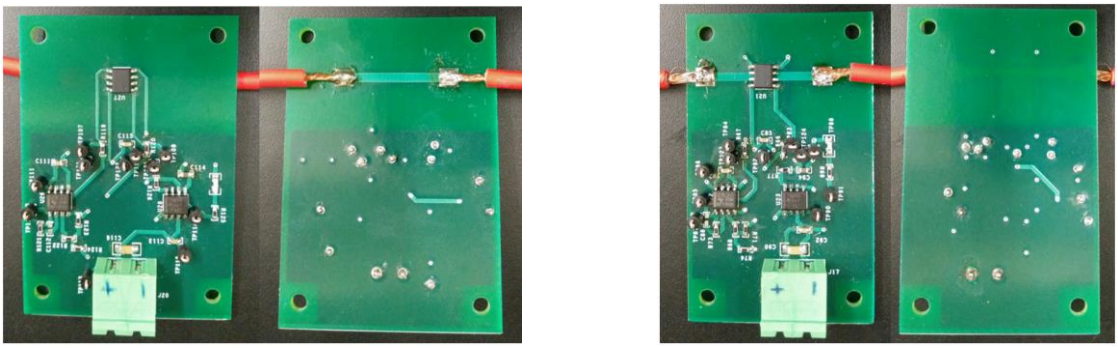

(a) (b)

Figure 3.6: GMR evaluation board with distance between sensor and the current trace (a) 2.32mm and (b) 0.75mm

The performance of the sensors are evaluated in terms of DC, AC and step currents. The AMR prototype board was exposed to a DC current varying from -10A to 10A whereas the GMR prototype board was evaluated with a DC current of 1A to 10A as the GMR sensor output is unipolar in nature. The response of both the AMR and GMR

sensors are recorded and compared. Figure 3.7 and Figure 3.8 shows the response of the AMR and GMR sensor respectively with 2 different distance between the sensor and the current trace.

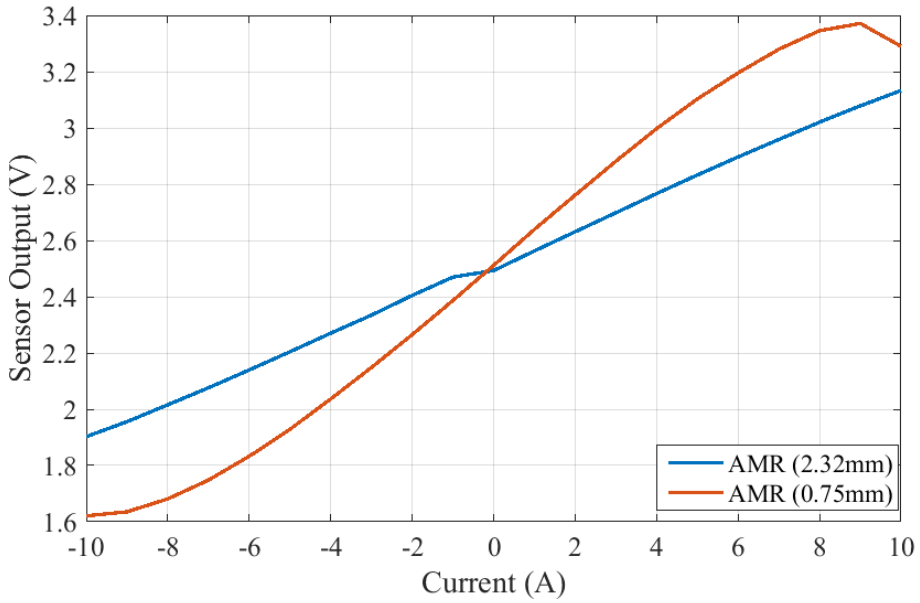

Figure 3.7: AMR response for DC currents from -10A to 10A

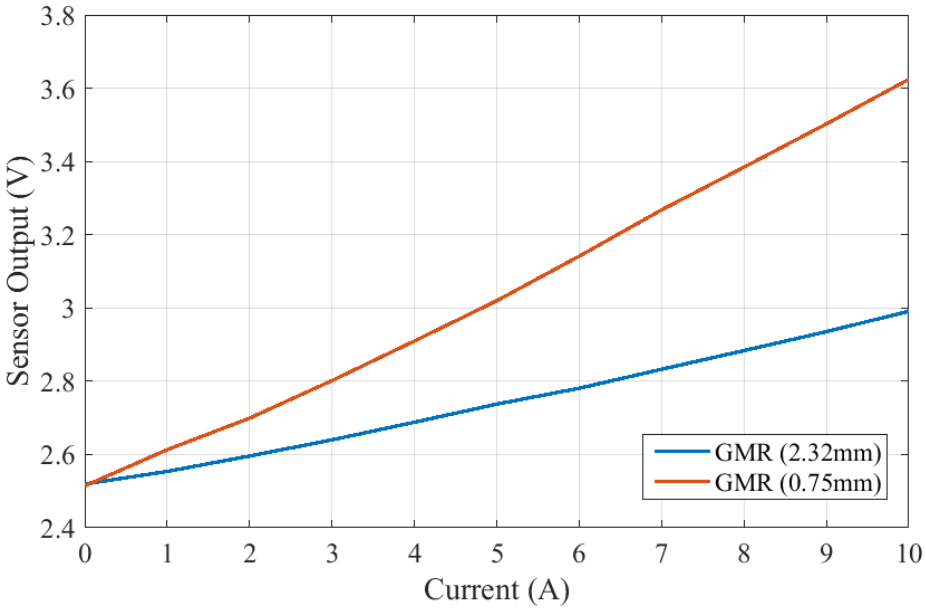

Figure 3.8: GMR response for DC currents from 0A to 10A

It can be observed that, both the AMR and GMR sensors respond linearly to DC currents within their sensing range. The response for both sensors is higher in case of 0.75mm distance between the sensor and the trace which is because of the higher magnetic field for shorter distance. For around 8A current and for the 0.75mm case, the AMR sensor response starts to fall down instead of increasing. This is because the calculated magnetic field intensity for 8A for 0.75mm distance is 9.41Oe which is almost close to the boundary of linear range of operation of 10 Oe for AMR sensor. The GMR sensor output shows no sign of saturation even at 10A current as the sensing range for the selected sensor is up to 14 Oe. The calculated sensitivity from the DC current response test for the selected AMR sensor for 2.32mm and 0.75mm distance are 9.41 mV/V/mT and 10.05 mV/V/mT respectively. Whereas for GMR sensor the sensitivity is calculated to be 15.35 mV/V/mT and 22.32 mV/V/mT respectively. The experimentally calculated sensitivities are in well accordance to the manufacture specified sensitivity values.

For performance characterization in terms of AC currents, an inverter running with 26kHz switching frequency was utilized to generate a 60Hz sinusoidal current output of 3A(rms). The designed prototype sensor boards are exposed to the AC current and the response of the sensors are observed. Figure 3.9 and Figure 3.10 shows the scope captures of the AMR and GMR sensor response. It is clear from Figure 3.10 that, the GMR sensor has a unipolar output, hence the rectified output for a sinusoidal input current. The AMR sensor on the other hand is bipolar are is able to respond to the alternating field accordingly. The GMR response for positive and negative half cycle of the reference current is not identical and negative half cycle is showing slightly higher

output that the positive half cycle. This can be explained by the hysteresis curve of the GMR element which is not symmetrical along the 0 magnetics field line.

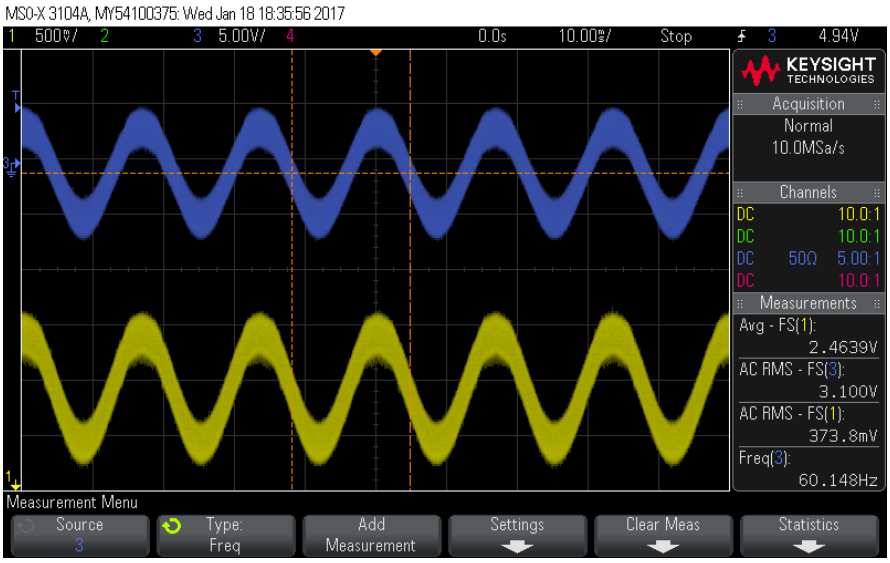

Figure 3.9: AMR sensor response for 3A (rms) AC current with 0.75mm distance between the sensor and trace

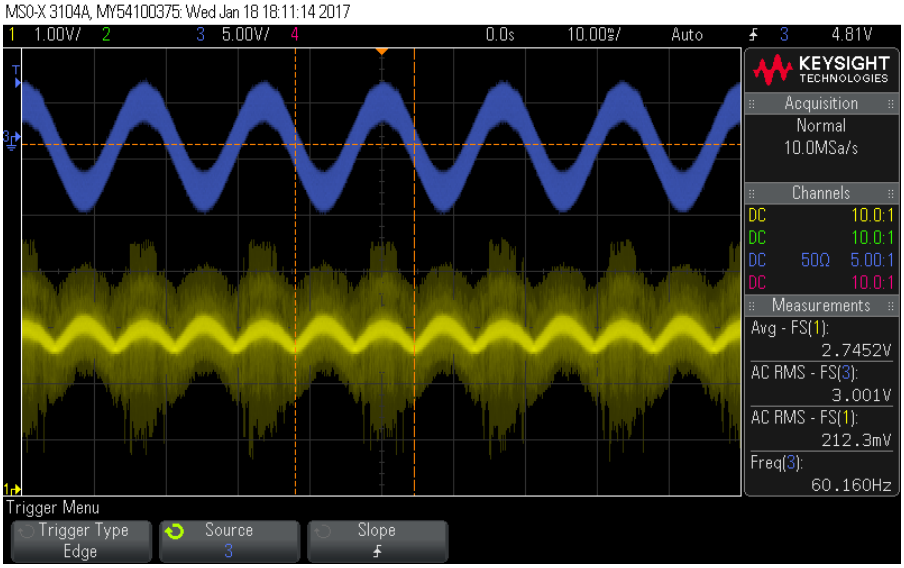

Figure 3.10: GMR sensor response for 3A (rms) AC current with 0.75mm distance between the sensor and trace

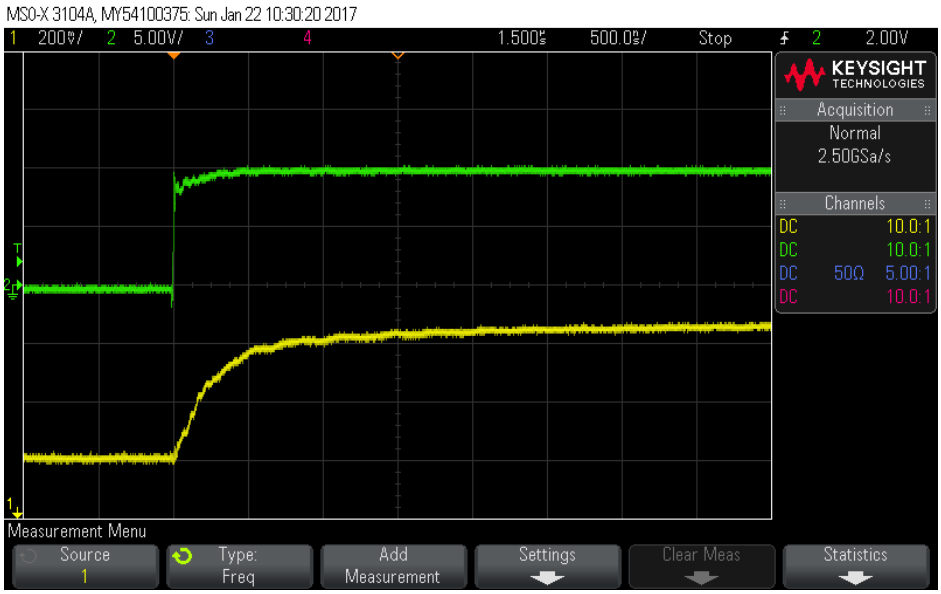

Figure 3.11: AMR sensor response for 10A step current

Figure 3.12: GMR sensor response for 10A step current

Lastly, the sensors were exposed to a 10A current step to evaluate the performance with respect to a step current. A custom designed high rise step current generator was used for the generation of the 8ns fast rise 10A current step. For this

experiment, only the prototype boards having a 2.32mm distance between the sensor and the current trace were used, one each for AMR and GMR. The responses of the sensors with respect to a 10A step current are shown in Figure 3.11 and Figure 3.12. It is clear from the figures that the GMR sensor is able to respond to the fast rise 10A transient compared to the AMR sensor. The experimental results and data were exported to MATLAB for further analysis.

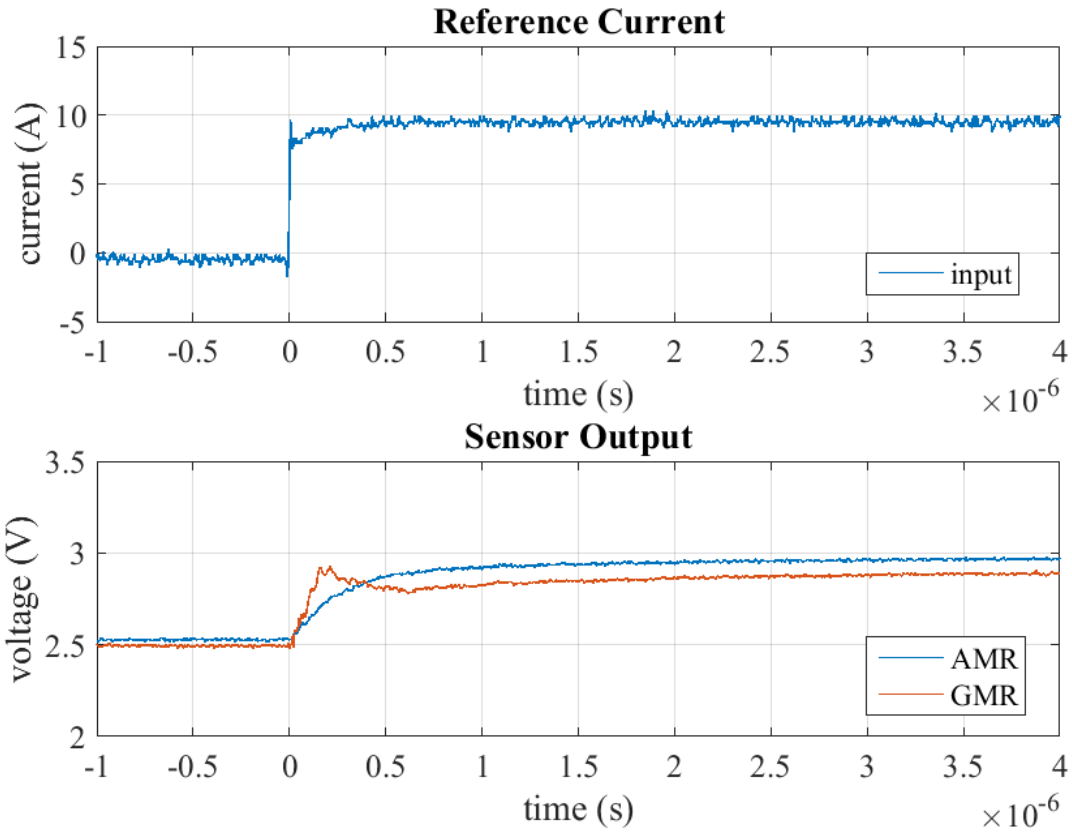

Figure 3.13: AMR and GMR sensor response for a fast 10A step current

Figure 3.13 shows the time domain response of the AMR and GMR sensors plotted together. It is clear that although the steady state response of the GMR is slightly less than the AMR sensor, the GMR sensor is able to respond to the fast rise step current

much faster when compared with the AMR sensor. It should be noted that the, differential gain applied to the bridged outputs of the AMR and GMR sensors are 20 and 7.7 respectively. So, the raw bridge output of the GMR is much higher than the AMR. Figure 3.14 shows the frequency response of the results observed in Figure 3.13. It is clearly visible that the bandwidth of the GMR sensor is around 6MHz which is higher than the AMR sensor bandwidth of 1 MHz. This result corresponds to the faster response to the step current. Also, in the phase diagram of Figure 3.14 we can see that the GMR sensors phase is holding constant for a much higher frequency when compared with AMR sensor phase response.

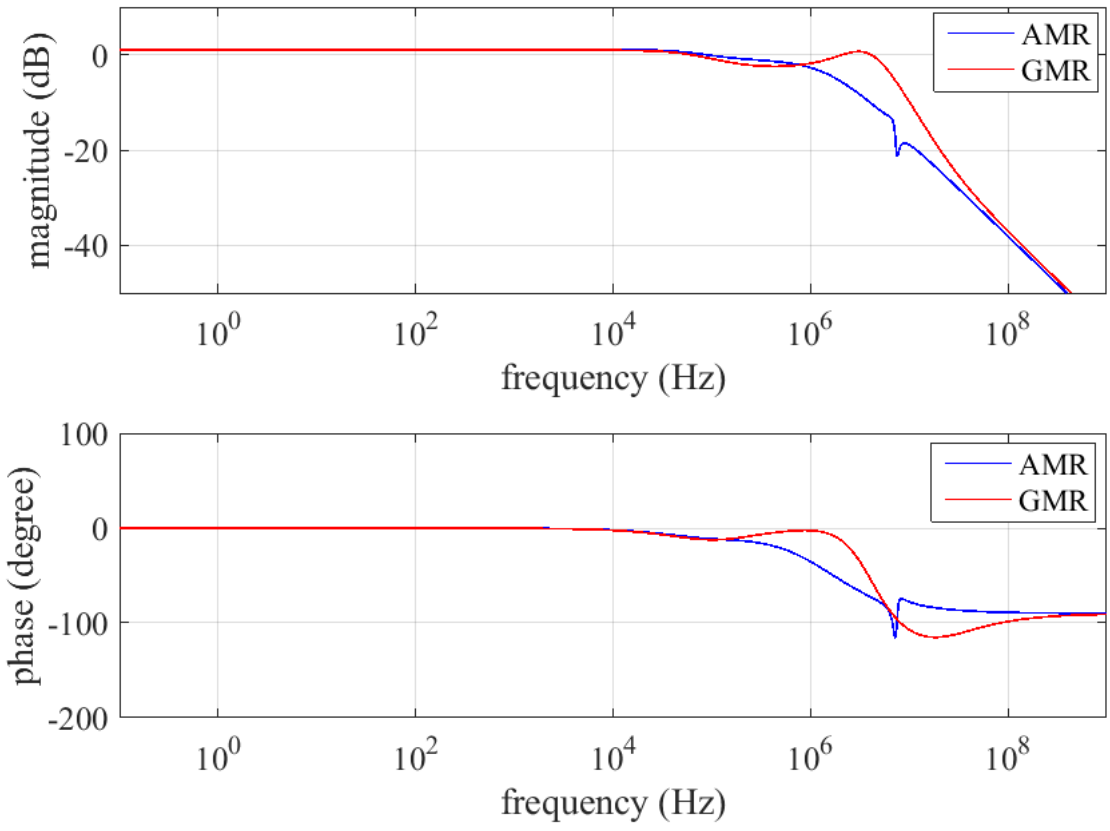

Figure 3.14: Frequency response for the step current response presented in Figure 3.13

3.3 Conclusion

This chapter presented a detailed characterization of two different commercially available Anisotropic Magnetoresistor (AMR) and Giant Magnetoresistor (GMR) sensors in terms of isolated and contactless current measurement in power electronic applications. The test circuits for the experiment are designed on a 4-layer PCB and 4 different test boards are realized for experiments. The sensors are evaluated at two different distances from the PCB current trace. The sensor performances are analyzed in terms of both DC and AC currents and results are presented accordingly. Both the AMR and the GMR sensor showed linear response within their respective sensing range. The AMR sensor has a bipolar output compared to the GMR which is unipolar and provided a rectified output for sinusoidal AC current. However, both sensors are capable of responding to the AC fields and to the inductor ripple currents of the DC-AC inverter output. The sensitivity of the AMR and GMR sensors are calculated and verified. The sensors are evaluated with respect to a fast rise step current generator to analyze the bandwidth of sensing. The GMR sensor response shows a higher bandwidth than the AMR sensor with respect to a fast step current response.

CHAPTER 4: ENHANCED BANDWIDTH CONTACTLESS CURRENT SENSING USING MAGNETORESISTIVE SENSORS FOR POWER ELCETRONIC APPLICATIONS

Current information is the most essential parameter for control, diagnostic and prognostic purposes. The miniaturization of high-power electronics generates electromagnetic interference (EMI) between the current traces, the IC, and various components on the circuit board. The introduction of smarter power generation devices, which include current monitoring sensors, brought to light one of the main challenges of high power circuit design, namely, that EMI interferes with the current monitoring circuit and is detrimental to the performance of the electronics if not controlled. The generation of EMI and its interaction with locally placed components are currently not well understood. To advance the understanding of how to mitigate the effects of EMI in high power electronics, there is a need to investigate alternative approaches and techniques to measure current. The aim is to develop current sensors that respond quickly and are accurate and loss-less. Moreover, the increased application of high voltage devices (>30V) using Wide-Bandgap (WBG) semiconductors in high frequency power converters (>1MHz) requires isolated current sensors.

Emergence of next generation power semiconductor switches and new technologies in power electronics, researchers are pushing the boundary of efficiency and control to a new level [108]-[117]. The advanced control algorithms as well as the efficiency and power density demands of designers call for accurate measurement of

current information in the power electronics converter. Different integrated and lossless current sensing methods, such as series MOSFET's on-resistance and parallel current-sensing FET (sense-FET) have been proposed to deduce the switch or inductor current information. However, these approaches do not provide electric isolation and are limited to low voltage applications. Among many different types of isolated sensors, magnetic field induction-based transducers and Hall-effect sensors are among the most popular technologies, and significant performance improvements have been made over the past years.

Typical Si-based Hall sensors have bandwidth limited to only tens of kilohertz. Using materials with higher carrier mobility than Si, such as GaAs and InAs, allows the element's thickness reduction while increasing its sensitivity and ability to detect faster transients up to 1 MHz. Due to the emergence of high frequency power converters (>1MHz), there is a need to develop other methods to detect such high frequency currents.

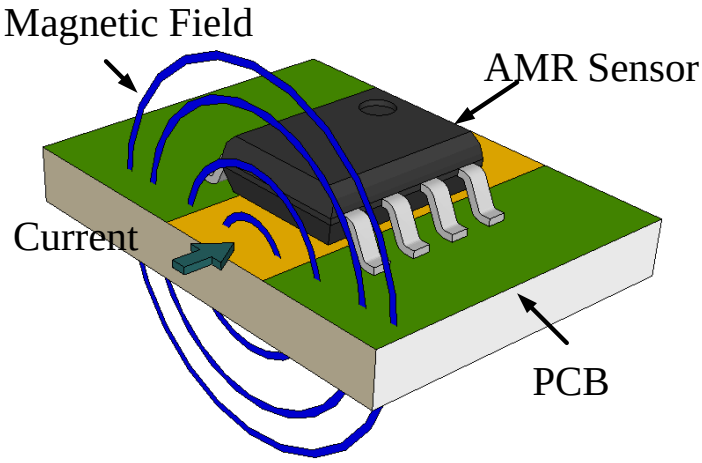

Figure 4.1: Standard configuration of AMR sensor for current measurement

Hall-effect and magnetoresistive devices can detect both DC and AC fields. Whereas Hall-effect sensors are made of semiconductors, magnetoresistive sensors can be fabricated from both semiconductors and metal alloys. This permits the conductivity and the sensitivity to be tailored precisely to the application. In contrast to Hall-effect sensors, magnetoresistive sensors do not suffer from drift and are less susceptible to external noise, increasing their utility for application in high frequency power electronics. While MRs are based on low bandgap semiconductors, such as InSb and InAs, AMRs are based on metal alloys. The most widely used AMR device developed and integrated into a chip is composed of four Permalloy (Ni0.81Fe0.19) AMRs in a full sensitivity Wheatstone bridge configuration [67].

In a general power electronic application, the MR-based current sensor is placed on top or underneath a printed circuit board trace carrying the current without any conductive contact to the trace. Figure 4.1 shows the "standard configuration" and necessary layout for an AMR sensor IC to measure the current. The sensor detects the magnetic field generated by the current carrying power PCB trace. At low frequencies, the magnetic field around the trace is uniformly distributed and intersects the sensor along the default axis generating a response. However, at higher frequencies, especially above 1 MHz, due to the skin effect, the current tends to flow mostly on the edges of the PCB trace. As a result, the generated magnetic field distribution is not uniform and is mostly concentrated around the edges. Unfortunately, the AMR current sensor detects the weaker part of field distribution over the frequency of operation, giving the false impression that it loses its sensitivity at higher frequencies. Consequently, its application is limited to much less than 1 MHz. Normalizing the magnetic field over the frequency

range of interest with magnetic concentrators, results in an increase in the detected bandwidth and sensitivity of the sensor. These magnetic concentrators maximize the magnetoresistive sensor's bandwidth. The concept of using magnetic concentrators as a method of increasing the sensitivity of devices has already been established for Hall-effect based devices using ferromagnetic materials [64]-[65].

In this chapter, we propose a method to increase the sensitivity and frequency bandwidth of MR sensors, specifically, AMR sensors, enabling the detection of current with very fast transients. The approach presented in this chapter concentrates and normalizes the magnetic field induced by the wideband current in PCB traces commonly seen in power electronics applications. Section 4.1 details the proposed method to increase the detected bandwidth of the AMR sensor. It is followed by the experimental verification of the proposed method which is presented in section 4.2. Section 4.3 summarizes the findings and conclusions.

4.1 Proposed Method for Wideband Current Measurements

The magnetic field distribution around the current trace is significantly non-uniform at high frequencies due to the skin effect. This means that point-field detectors such as AMR sensors need to be placed accurately where the respective radiated magnetic field can be measured uniformly over the bandwidth of interest i.e. DC-5MHz. In other words, the general scheme shown in Figure 4.1 may not be used for wideband current measurements, and proper magnetic field concentration technique is required for sensing the high frequency current.

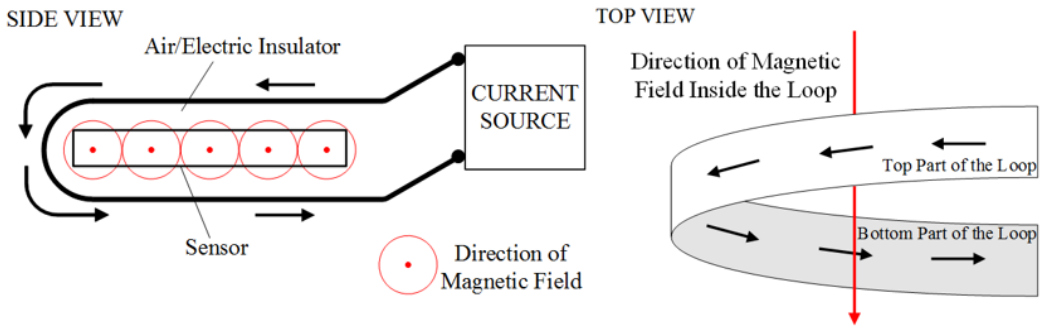

Figure 4.2: Proposed folded trace technique to normalize and intensify the field

The proposed method addresses these challenges by modifying the layout of the current trace carrying the current to be detected and combining it with a sensitive AMR sensor. By wrapping the current trace around the top and the bottom of the AMR sensor, the magnetic field detected by the sensor becomes uniform in the frequency range of interest. The proposed method generates a much more uniform magnetic field, whose magnitude depends on the current, along the sensitive axis of the sensor. The proposed method is visualized in Figure 4.2.

To better understand the distribution of magnetic field around the bare trace and the proposed folded trace, a set of simulations are provided using a full-wave commercial electromagnetic solver, Ansys HFSS. The simulations include copper traces with dimensions of 10mm and 5mm along the X and Y axes, respectively, and with a thickness of 35µm (equivalent to 1Oz copper) along the Z-axis. The folded trace technique has been implemented with 1.5mm gap between the two traces. Figure 4.3 presents the FEM simulation results for the bare and folded trace cases. By increasing the current's frequency from 100 kHz to 5 MHz, a much more uniform magnetic field distribution is obtained around the trace with the folded trace technique compared to the bare trace case. The difference in magnetic field distribution for 5 MHz frequency is

visible in the top-right and bottom-right figures in Figure 4.3. The field distribution in between the two traces for the bottom-right figure is much more uniform compared to the one with only a single bare trace.

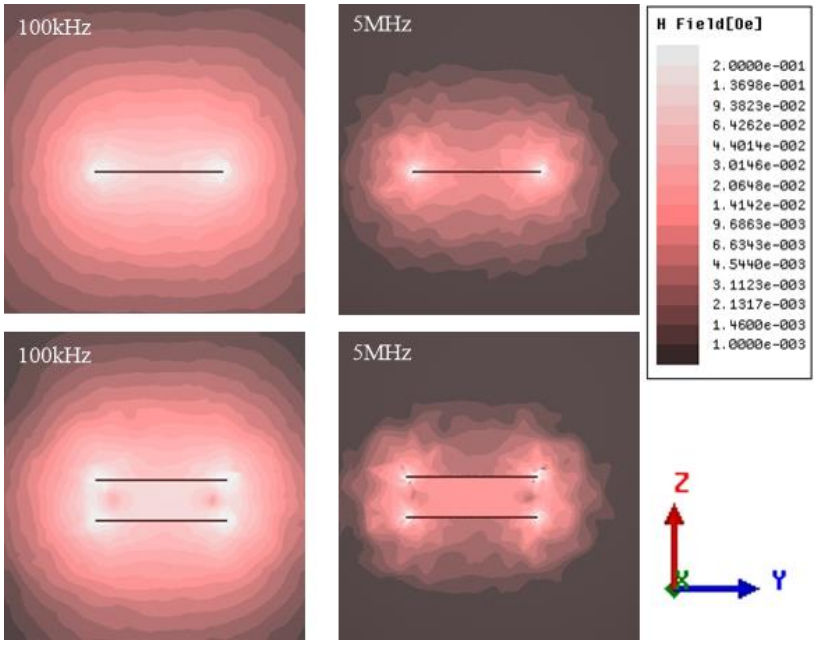

Figure 4.3: Simulation results: magnetic field distribution of bare trace (top) and folded trace (bottom) at two different frequencies

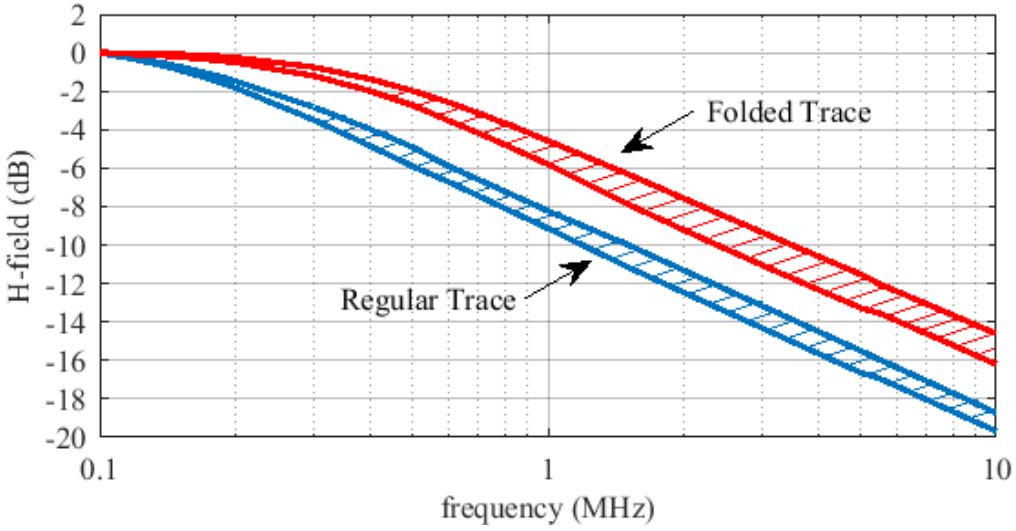

Figure 4.4: Normalized magnetic field distribution with respect to frequency for the simulations results in Figure 4.3 for different positions of the sensor element on the current carrying trace in regular and folded trace configuration

The simulation study is further carried out considering the relative position of the sensing element on top of the current trace. In this study, measurements have been taken for different positions around the trace going from the middle of the trace toward the edges where the magnetic field has the highest intensity, but is scattered and non-uniform. Consequently, the area from the middle of the trace to around 2/3 of the distance toward the edge is the area that has a positive effect on the sensitivity of the sensor. The simulated results for the change in magnetic field distribution within this area with respect to different frequencies for both bare trace and folded trace configurations are presented in Figure 4.4. The captured H-field data from the simulations with respect to the change in frequency varying from 100 kHz to 10 MHz is normalized for each case shown in Figure 4.4. The proposed folded trace method has an overall improved magnetic flux distribution in terms of uniformity and intensity.

It is also worth mentioning that the proposed method concentrates the magnetic field onto the current sensor without altering the current on the trace and simultaneously shields the sensor from any other stray magnetic fields, which are very common in switching power converters.

4.2 Experimental Verification of the Proposed Method

To examine the performance of the AMR-based current sensor, several circuits were designed and implemented. Figure 4.5 presents the circuit diagram of the hardware setup designed to evaluate the performance of the proposed method. To evaluate the bandwidth of the current sensor in a timely manner, a fast high-rise current step function generator was used. The step current was obtained by charging a capacitor bank and then

discharging it through a small power resistor. The voltage across the resistor was taken as the reference current measurement, as shown in the left side circuit in Figure 4.5. Subsequently, a current sensing scheme using a commercially available AMR sensor was designed and developed [67]. The sensor output was amplified by a differential amplifier with a gain of 50. The right side circuit of Figure 4.5 shows the sensor and signal conditioning circuit.

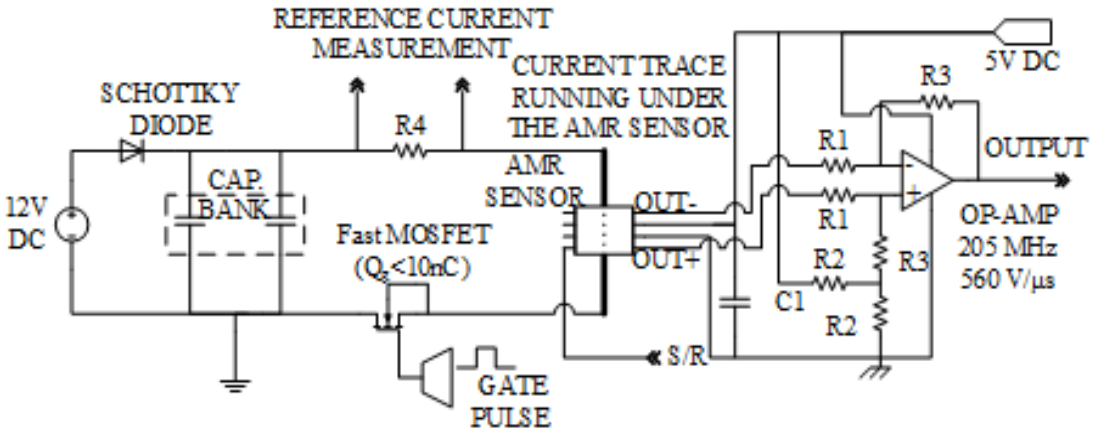

Figure 4.5: Circuit diagram of the set-up for testing the AMR sensing scheme

Figure 4.6 shows the hardware prototype developed for the experiment with the standard configuration (left) and the proposed folded trace configuration (right). The current carrying trace with 1Oz copper is implemented on the bottom layer of the PCB with 1.5mm thickness as shown in Figure 4.6-left picture. Copper foil with 35µm (1Oz) thickness is used to implement the proposed folded trace covering the AMR sensor. The main signal conditioning circuit is designed with high speed components (205MHz, 506V/µs) such that it does not limit the frequency range of interest. Figure 4.6-right

presents the picture of the hardware prototype that was fabricated to study the AMR sensor with the proposed method.

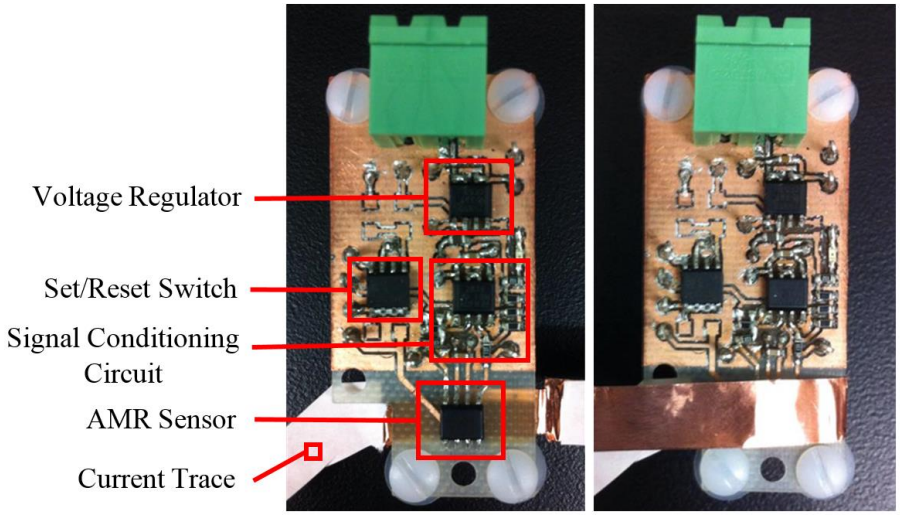

Figure 4.6: Hardware setup for evaluation of the AMR current sensor. Left: standard scheme, Right: sensing scheme with the folded trace technique

Figure 4.7 presents the experimental results captured from our prototype testing with the bare/regular trace and the proposed folded trace. Data collected from the prototype revealed that the detected voltage signal in the "folded trace" configuration is amplified compared to the "standard configuration", in which the sensor is positioned over the current trace. In other words, it can be concluded that the sensor with the proposed method has an improved sensitivity compared to the standard configuration.

It is also clear from Figure 4.7 that the AMR sensor in the folded trace configuration follows the reference current significantly better than in the standard configuration. During the characterization of the AMR sensor in the vicinity of a current carrying PCB trace with standard configuration, initially the sensor output behaves completely out of phase at very high frequencies. Based on that result, one might not expect the AMR sensor to be capable of following a very high frequency magnetic field.

The sensor output is expected to behave like a first-order system. The reason for such behavior of the sensor can be explained by the simulation results of Figure 4.3 with bare trace having non-uniform magnetic field distribution around the current trace. The scattered magnetic field causes the AMR elements to align in different directions generating out-of-phase response from the sensor. This behavior is unique to AMRs and needs further study by modeling the AMR element in terms of frequency over the range of detection. Nonetheless, the results obtained from the experiment using the proposed method show that by amplification and normalization of the field at the sensor's sensitive axis (easy axis), it is possible to achieve higher sensitivity over the linear region of the point-field detector, in this case, AMR. This amplification can also be observed by comparing the steady-state response (low frequency) of the AMR in the "folded trace" with the "standard" configurations (Figure 4.7).

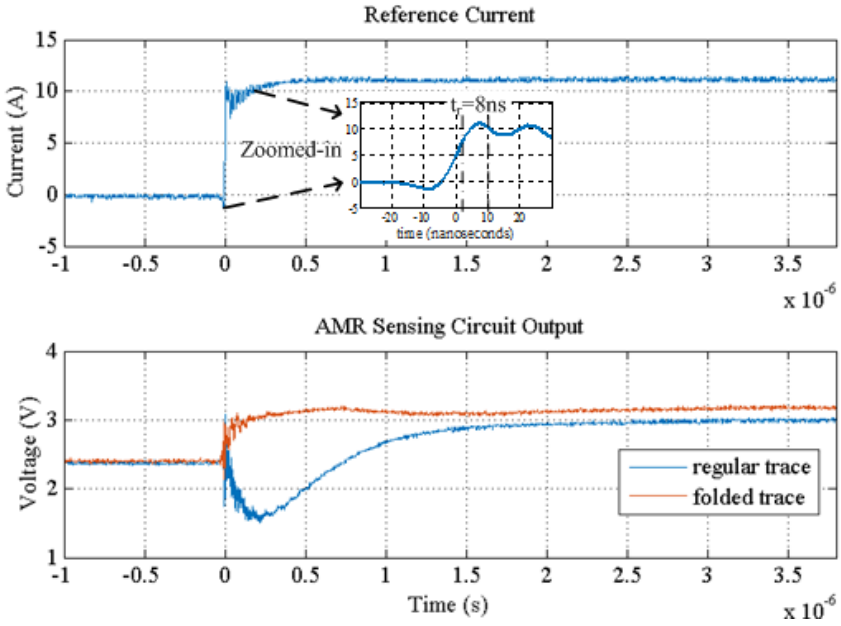

Figure 4.7: Experimental Results: step response comparison of the AMR sensing circuit for regular trace and the proposed folded trace implementation

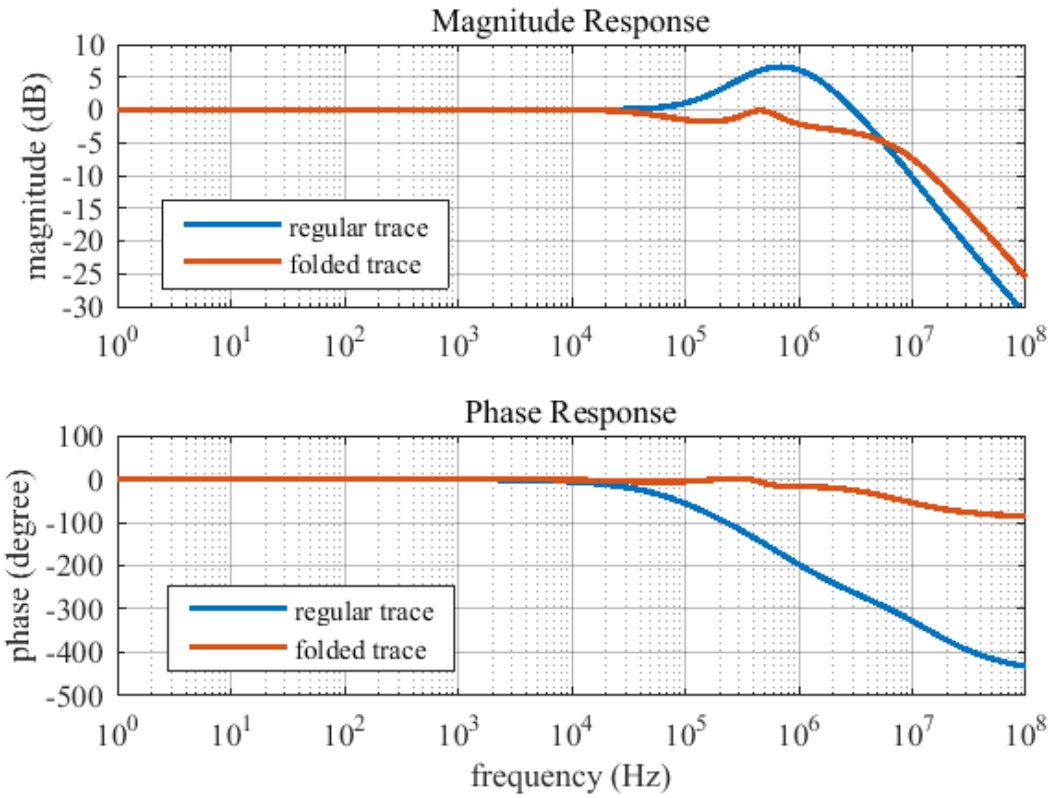

Figure 4.8: Frequency analysis (normalized) of AMR sensor with Regular (Bare) Trace and Folded Trace based on the experimental results shown in Figure 4.7

Figure 4.8 presents the frequency response analysis of the normalized experimental data shown in Figure 4.7. The difference in detection bandwidth for the sensor is clearly visible in the magnitude response plot. The gain magnitude for the proposed folded trace method remains more stable for a much higher frequency range compared to the bare trace configuration. More importantly, if we look at the phase response, in case of the standard bare trace configuration, the phase begins to deviate at about 20 kHz. As we approach 1 MHz frequency, the phase becomes completely out of phase, which is in accordance with the out-of-phase response we have observed in Figure 4.7. The proposed folded trace method remains fairly constant until 5 MHz. For high frequency applications in the megahertz range, the AMR sensor exposed to a bare current

trace has a slightly higher gain, but the out-of-phase behavior of the sensor response means that the sensor is not able to react to high frequency magnetic fields properly. The proposed method to amplify and make the magnetic field more uniform results in the AMR elements responding in phase and accurately to currents at higher frequencies.

These results lead us to conclude that 1) if the magnetic field is large enough and uniform over frequency, the AMR sensor can detect MHz changes, unlike Hall elements, and 2) isolated magnetic concentrators, such as the proposed folded trace, improve the performance and response time of the AMR elements when they are used as contactless current sensors.

4.3 Conclusion

In this chapter, we have proposed a technique for an AMR-based sensing circuit that allows current measurements over a wide frequency range. This is accomplished by folding the current carrying trace around the AMR sensor to amplify and normalize the magnetic field generated by the current over a wide frequency range. The experimental results show that the sensor, when implemented with the proposed method, has an improved bandwidth of up to 5 MHz and enhanced sensitivity to high frequency currents evinced by the sensor output at DC. It is believed that the proposed method is applicable in high frequency power converters where the inductor current is used to control the ripple and transient response.

CHAPTER 5: CONCLUSION AND FUTURE WORK

Current sensing techniques for high frequency power converters should yield to have some key characteristics such as – fast, accurate, isolated, loss-less and most importantly wide bandwidth. In this research, a detailed review of different traditional and advanced current measurement techniques has been performed. Starting from the very basic sense resistors to the most advanced wideband hybrid sensing technologies, each method offers its own advantages while having some limitations. Keeping in mind the future integration possibility of these current sensors in the high frequency power modules, isolated and loss-less current sensing techniques such as Hall-effect and Magnetoresistors provide the most efficient solution for current measurement in power converters. Magnetoresitive sensors has the advantage of responding to horizontal magnetic fields compared to the Hall-effect sensors which respond to the vertical components of the magnetic field. The sensing bandwidth of the MR sensors are much higher than the Hall-effect sensors which makes it an ideal candidate for applications such as high frequency power converters.

Anisotropic Magnetoresistors (AMR) and Giant Magnetoresistors (GMR) are two of the most popular variants of magnetoresistor elements that are used as current sensors. In this study, a detailed characterization of these elements are performed with respect to DC, AC and step currents. Both the AMR and the GMR sensor showed linear response within their respective sensing range. The AMR sensor has a bipolar output compared to

the GMR which is unipolar and provided a rectified output for sinusoidal AC current. The sensitivity of the AMR and GMR sensors are calculated and experimentally verified. The AMR and GMR sensors are evaluated with respect to a fast rise step current generator to analyze the bandwidth of sensing. The GMR sensor response shows a higher bandwidth than the AMR sensor with respect to a fast step current response. The MR sensors are magnetic point field detectors which are sensitive to any magnetic fields present in the vicinity of the sensor and experimental setup. Hence, the performance of the sensing accuracy and response varies with changes prototypes and basic experimental setup.

Finally, a novel technique for an AMR-based sensing circuit has been proposed in this study which allows current measurements over a wide frequency range. This is achieved by folding the current trace on top of the AMR sensor for the purpose of intensifying and normalizing the magnetic field over the frequency range of interest. The concept has been verified by advanced simulations run in a full wave electromagnetic solver Ansys HFSS. The folded trace concept is tested with distinctly developed porotype circuits and verified experimentally by specific setup of the sensor and prototypes. The sensor, when implemented with the proposed method, shows an improved bandwidth of up to 5 MHz and enhanced sensitivity to high frequency currents. It is believed that the proposed method is applicable in high frequency power electronic converters, where the inductor current is used to control the ripple and transient response.

REFERENCES

[1] S. Ziegler, R. C. Woodward, H. H. C. Iu and L. J. Borle, "Current Sensing Techniques: A Review," in IEEE Sensors Journal, vol. 9, no. 4, pp. 354-376, April 2009.

[2] A. Patel and M. Ferdowsi, "Current Sensing for Automotive Electronics—A Survey," in IEEE Transactions on Vehicular Technology, vol. 58, no. 8, pp. 4108-4119, Oct. 2009.

[3] H. P. Forghani-zadeh and G. A. Rincon-Mora, "Current-sensing techniques for DC-DC converters," The 2002 45th Midwest Symposium on Circuits and Systems, 2002. MWSCAS-2002., 2002, pp. II-577-II-580 vol.2.

[4] Chucheng Xiao, Lingyin Zhao, T. Asada, W. G. Odendaal and J. D. van Wyk, "An overview of integratable current sensor technologies," 38th IAS Annual Meeting on Conference Record of the Industry Applications Conference, 2003., 2003, pp. 1251-1258 vol.2.

[5] A. M. Patel and M. Ferdowsi, "Advanced Current Sensing Techniques for Power Electronic Converters," 2007 IEEE Vehicle Power and Propulsion Conference, Arlington, TX, 2007, pp. 524-530.

[6] M. Biglarbegian, S. J. Nibir, H. Jafarian and B. Parkhideh, "Development of current measurement techniques for high frequency power converters," 2016 IEEE International Telecommunications Energy Conference (INTELEC), Austin, TX, 2016, pp. 1-7.

[7] J. A. Ferreira, W. A. Cronje and W. A. Relihan, "Integration of high frequency current shunts in power electronic circuits," Power Electronics Specialists Conference, 1992. PESC '92 Record., 23rd Annual IEEE, Toledo, 1992, pp. 1284-1290 vol.2.

[8] J. A. Ferreira, W. A. Cronje and W. A. Relihan, "Integration of high frequency current shunts in power electronic circuits," in IEEE Transactions on Power Electronics, vol. 10, no. 1, pp. 32-37, Jan 1995.

[9] F. Castelli, "The flat strap sandwich shunt," in IEEE Transactions on Instrumentation and Measurement, vol. 48, no. 5, pp. 894-898, Oct 1999.

[10] B. Mammano, “Current-sensing solutions for power-supply designers,” in Unitrode Design Note. Dallas, TX: Texas Instruments, 1997.

[11] L. Hua, S. Luo, “Design Considerations of Time Constant Mismatch Problem for Inductor DCR Current Sensing Method,” IEEE Applied Power Electronics Conf. Proc. (APEC), 2006, pp.1368-1374.

[12] L. Hua, S. Luo, “Design Considerations for Small Signal Modeling of DC-DC Converters Using Inductor DCR Current Sensing Under Time Constants Mismatch Conditions,” IEEE Power Electronics Specialists Conf. Proc. (PESC), 2007, pp.2182-2188.

[13] A. T. Mozipo, "Analysis of a current sensing and reporting tolerance in an inductor DCR sense topology," 2011 Twenty-Sixth Annual IEEE Applied Power Electronics Conference and Exposition (APEC), Fort Worth, TX, 2011, pp. 1502-1506.

[14] Giorgio Spiazzi, Simone Buso, and Luca Corradini, “Dynamic Effects of Mismatched Time Constants in DC-DC Converters with Inductor DCR Current Sensing”, IEEE Energy Conversion Congress and Exposition (ECCE), 2014.

[15] Z. Lukic, S. M. Ahsanuzzaman, A. Prodic and Z. Zhao, "Self-Tuning Sensorless Digital Current-Mode Controller with Accurate Current Sharing for Multi-Phase DC-DC Converters," 2009 Twenty-Fourth Annual IEEE Applied Power Electronics Conference and Exposition, Washington, DC, 2009, pp. 264-268.

[16] A. Simon-Muela, S. Petibon, C. Alonso, B. Estibals, L. Seguier and J. L. Chaptal, "Practical Implementation of a High-Frequency Current Sensing Technique for VRM," 2007 IEEE International Symposium on Industrial Electronics, Vigo, 2007, pp. 764-769.

[17] S. Yuvarajan and L. Wang, "Performance analysis and signal processing in a current sensing power MOSFET (SENSEFET)," Conference Record of the 1991 IEEE Industry Applications Society Annual Meeting, Dearborn, MI, USA, 1991, pp. 1445-1450 vol.2.

[18] H. Lavric and R. Fiser, "Lossless current sensing technique on MOSFET RDS(on) with improved accuracy," in Electronics Letters, vol. 46, no. 5, pp. 370-371, March 4 2010.

[19] O. Aiello and F. Fiori, "Current sensing circuit for DC-DC converters based on the miller effect," 2013 International Conference on Applied Electronics, Pilsen, 2013, pp. 1-4.

[20] H. Forghani-zadeh, “An Integrated, Lossless, and Accurate Current-Sensing Technique for High-Performance Switching Regulators,” Ph.D. Dissertation, Georgia Institute of Technology, Aug. 2006.

[21] P. Liu, L. Zhang, A. Q. Huang, S. Guo and Y. Lei, "High bandwidth current sensing of SiC MOSFET with a Si current mirror," 2016 IEEE 4th Workshop on Wide Bandgap Power Devices and Applications (WiPDA), Fayetteville, AR, 2016, pp. 200-203.

[22] Y. Wen, M. Rose, R. Fernandes, R. Van Otten, H. J. Bergveld and O. Trescases, "A Dual-Mode Driver IC With Monolithic Negative Drive-Voltage Capability and Digital Current-Mode Controller for Depletion-Mode GaN HEMT," in IEEE Transactions on Power Electronics, vol. 32, no. 1, pp. 423-432, Jan. 2017.

[23] A. Furukawa et al., "Low on-resistance 1.2 kV 4H-SiC MOSFETs integrated with current sensor," 2011 IEEE 23rd International Symposium on Power Semiconductor Devices and ICs, San Diego, CA, 2011, pp. 288-291.

[24] "Current Sensing Power MOSFETs," AND8093/D, On Semiconductor, Application Notes, Mar. 2017, Rev. 6.

[25] E. R. Motto, and J. F. Donlon, "New compact IGBT modules with integrated current and temperature sensors," Powerex technical library, 2005.

[26] "Current Sensing Power MOSFETs," AN10322, Nexperia Semiconductor, Application Notes, Jun. 2009, Rev. 2.

[27] J. Steele, "Current Sensing for Server Power Monitoring: MOSFET Or Shunt?", Power Electronics Technology, National Semiconductor, Jul. 2011.

[28] Current Sense Transformers CST7030, Coilcraft, Datasheet, 2015, [Online], Available: http://www.coilcraft.com/pdfs/cst7030.pdf.

[29] Current Sense Transformers CST4835, Coilcraft, Datasheet, 2016, [Online], Available: http://www.coilcraft.com/pdfs/cst4835.pdf.

[30] Leung-Pong Wong, Yim-Shu Lee and David Ki-Wai Cheng, "Bi-directional pulse-current sensors for bi-directional PWM DC-DC converters," 2000 IEEE 31st Annual Power Electronics Specialists Conference. Conference Proceedings (Cat. No.00CH37018), Galway, 2000, pp. 1043-1046 vol.2.

[31] I. M. Filanovsky and V. A. Piskarev, "Sensing and measurement of DC current using a transformer and RL-multivibrator," in IEEE Transactions on Circuits and Systems, vol. 38, no. 11, pp. 1366-1370, Nov 1991.

[32] Kwok-Wai Ma and Yim-Shu Lee, "Technique for sensing inductor and DC output currents of PWM DC-DC converter," in IEEE Transactions on Power Electronics, vol. 9, no. 3, pp. 346-354, May 1994.

[33] K. W. Ma and Y. S. Lee, "Novel, technique for sensing inductor current and DC output current of PWM DC-DC converter," Applied Power Electronics Conference and Exposition, 1992. APEC '92. Conference Proceedings 1992., Seventh Annual, Boston, MA, 1992, pp. 345-351.

[34] N. McNeill, N. K. Gupta and W. G. Armstrong, "Active current transformer circuits for low distortion sensing in switched mode power converters," in IEEE Transactions on Power Electronics, vol. 19, no. 4, pp. 908-917, July 2004.

[35] Yan-Fei Liu and P. K. Jain, "A new current sensing scheme for zero-voltage switching phase-shifted bridge converter," INTELEC. Twenty-Second International Telecommunications Energy Conference (Cat. No.00CH37131), Phoenix, AZ, 2000, pp. 567-573.

[36] Jian Yang and Lei Hua, "Analysis and design consideration of using current sensing transformer in forward converter with synchronous rectification," Applied Power Electronics Conference and Exposition, 2004. APEC '04. Nineteenth Annual IEEE, 2004, pp. 878-882 vol.2.

[37] K. Jin, L. Gu, Y. Sun and M. Xu, "A Current-Sensing Method for Integrated Transformer," in IEEE Transactions on Power Electronics, vol. 27, no. 3, pp. 1061-1065, March 2012.

[38] L. Xu, Q. Chen, X. Ren, S. C. Wong and C. K. Tse, "Self-Oscillating Resonant Converter With Contactless Power Transfer and Integrated Current Sensing Transformer," in IEEE Transactions on Power Electronics, vol. 32, no. 6, pp. 4839-4851, June 2017.

[39] L. Xu, Q. Chen, X. Ren, S. Ping and S. C. Wong, "Self-oscillating contactless resonant converter with power transfer and current sensing integrated transformer," 2015 IEEE Energy Conversion Congress and Exposition (ECCE), Montreal, QC, 2015, pp. 4539-4543.

[40] W. F. Ray and C. R. Hewson, "High performance Rogowski current transducers," Conference Record of the 2000 IEEE Industry Applications Conference. Thirty-Fifth IAS Annual Meeting and World Conference on Industrial Applications of Electrical Energy (Cat. No.00CH37129), Rome, 2000, pp. 3083-3090 vol.5.

[41] B. Wang, D. Wang and W. Wu, "A Rogowski coil current transducer designed for wide bandwidth current pulse measurement," 2009 IEEE 6th International Power Electronics and Motion Control Conference, Wuhan, 2009, pp. 1246-1249.

[42] W. F. Ray, "Rogowski transducers for high bandwidth high current measurement," IEE Colloquium on Low Frequency Power Measurement and Analysis (Digest No. 1994/203), London, 1994, pp. 10/1-10/6.

[43] A. Radun and J. Rulison, "An alternative low-cost current-sensing scheme for high-current power electronics circuits," Conference Record of the 1990 IEEE Industry Applications Society Annual Meeting, Seattle, WA, USA, 1990, pp. 619-625 vol.1.

[44] A. Radun, "An alternative low-cost current-sensing scheme for high-current power electronics circuits," in IEEE Transactions on Industrial Electronics, vol. 42, no. 1, pp. 78-84, Feb 1995.

[45] J. D. Ramboz, "Machinable Rogowski coil, design, and calibration," in IEEE Transactions on Instrumentation and Measurement, vol. 45, no. 2, pp. 511-515, Apr 1996.

[46] J. D. Ramboz, "Machinable Rogowski coil, design and calibration," Instrumentation and Measurement Technology Conference, 1995. IMTC/95. Proceedings. Integrating Intelligent Instrumentation and Control., IEEE, Waltham, MA, USA, 1995, pp. 329-.

[47] I. A. Metwally, "Performance Improvement of Slow-Wave Rogowski Coils for High Impulse Current Measurement," in IEEE Sensors Journal, vol. 13, no. 2, pp. 538-547, Feb. 2013.

[48] A. M. Luciano and M. Savastano, "Wide band transformer based on a split-conductor current sensor and a Rogowski coil for high current measurement," Instrumentation and Measurement Technology Conference, 1995. IMTC/95.

[49] Si85XX unidirectional AC current sensors, Silicon Labs, Datasheet, 2012, [Online], Available: https://media.digikey.com/pdf/Data%20Sheets/Silicon%20Laboratories%20PDFs/SI85xx_C_Rev2012_DS.pdf

[50] R. Y. Han et al., "Hybrid PCB Rogowski Coil for Measurement of Nanosecond-Risetime Pulsed Current," in IEEE Transactions on Plasma Science, vol. 43, no. 10, pp. 3555-3561, Oct. 2015.

[51] N. Karrer and P. Hofer-Noser, "PCB Rogowski coils for high di/dt current measurement," 2000 IEEE 31st Annual Power Electronics Specialists Conference. Conference Proceedings (Cat. No.00CH37018), Galway, 2000, pp. 1296-1301 vol.3.

[52] L. Zhao, J. D. van Wyk and W. G. Odendaal, "Planar embedded pick-up coil sensor for power electronic modules," Applied Power Electronics Conference and Exposition, 2004. APEC '04. Nineteenth Annual IEEE, 2004, pp. 945-951 vol.2.

[53] Y. Xue, J. Lu, Z. Wang, L. M. Tolbert, B. J. Blalock and F. Wang, "A compact planar Rogowski coil current sensor for active current balancing of parallel-

connected Silicon Carbide MOSFETs," 2014 IEEE Energy Conversion Congress and Exposition (ECCE), Pittsburgh, PA, 2014, pp. 4685-4690.

[54] J. Wang, Z. Shen, C. DiMarino, R. Burgos and D. Boroyevich, "Gate driver design for 1.7kV SiC MOSFET module with Rogowski current sensor for shortcircuit protection," 2016 IEEE Applied Power Electronics Conference and Exposition (APEC), Long Beach, CA, 2016, pp. 516-523.

[55] J. Wang, Z. Shen, R. Burgos and D. Boroyevich, "Integrated switch current sensor for shortcircuit protection and current control of 1.7-kV SiC MOSFET modules," 2016 IEEE Energy Conversion Congress and Exposition (ECCE), Milwaukee, WI, 2016, pp. 1-7.

[56] High Speed Response Coreless Current Sensor, Asahi Kasei Micro-devices (AKM), Datasheet, 2015, [Online], Available: https://www.akm.com/akm/en/file/datasheet/CQ-3303.pdf.

[57] 1 MHz Bandwidth, Galvanically Isolated Current Sensor IC in Small Footprint SOIC8 Package, Allegro Microsystems, Datasheet, 2017, [Online], Available: https://www.allegromicro.com/~/media/Files/Datasheets/ACS730-Datasheet.ashx?la=en.

[58] P. D. Dimitropoulos, P. M. Drljaca and R. S. Popovic, "A 0.35um-CMOS, Wide-Band, Low-Noise HALL Magnetometer for Current Sensing Applications," 2007 IEEE Sensors, Atlanta, GA, 2007, pp. 884-887.

[59] J. Pankau, D. Leggate, D. W. Schlegel, R. J. Kerkman and G. L. Skibiniski, "High-frequency modeling of current sensors [of IGBT VSI]," in IEEE Transactions on Industry Applications, vol. 35, no. 6, pp. 1374-1382, Nov/Dec 1999.

[60] J. Pankau, D. Leggate, D. Schlegel, R. Kerkman and G. Skibiniski, "High frequency modeling of current sensors," Applied Power Electronics Conference and Exposition, 1999. APEC '99. Fourteenth Annual, Dallas, TX, 1999, pp. 788-794 vol.2.

[61] S. Reymond, P. Kejik and R. S. Popovic, "True 2D CMOS integrated Hall sensor," 2007 IEEE Sensors, Atlanta, GA, 2007, pp. 860-863.

[62] A. Ajbl, M. Pastre and M. Kayal, "A Fully Integrated Hall Sensor Microsystem for Contactless Current Measurement," in IEEE Sensors Journal, vol. 13, no. 6, pp. 2271-2278, June 2013.

[63] M. Banjevic, “High bandwidth CMOS magnetic sensors based on miniaturized circular vertical Hall devices,” Ph.D. dissertation, ´ Ecole Polytechnique F´ed´erale de Lausanne, Lausanne, Switzerland, 2011.

[64] R. S. Popovic, Z. Randjelovic, and D. Manic, “Integrated Hall-effect magnetic sensors,” Sens. Actuators A, Phys., vol. 91, pp. 46–50, Jun.2001.

[65] P. M. Drljaca, F. Vincent, P. Besse, and R. S. Popovic, “Design of planar magnetic concentrators for high sensitivity Hall devices,” Sens. Actuators A, Phys., vol. 97–98, pp. 10–14, Apr. 2002.

[66] IMC-Hall Current Sensor (Triaxis Technology), Melexis, Datasheet, 2015, [Online], Available: https://www.melexis.com/-/media/files/documents/datasheets/mlx91208-datasheet-melexis.pdf.

[67] 1-and 2-Axis Magn. Sens. HMC1001/1002/1021/1022, Honeywell (MN), Datasheet, 2008. [Online]. Available: http://www51.honeywell.com/aero/common/documents/myaerospacecatalog-documents/Missiles-Munitions/HMC_1001–1002–1021–1022_Data_Sheet.pdf.

[68] S. J. Nibir, E. Hurwitz, M. Karami and B. Parkhideh, "A Technique to Enhance the Frequency Bandwidth of Contactless Magnetoresistive Current Sensors," in IEEE Transactions on Industrial Electronics, vol. 63, no. 9, pp. 5682-5686, Sept. 2016.

[69] M. Biglarbegian, S. J. Nibir, H. Jafarian, J. Enslin and B. Parkhideh, "Layout study of contactless magnetoresistor current sensor for high frequency converters," 2016 IEEE Energy Conversion Congress and Exposition (ECCE), Milwaukee, WI, 2016, pp. 1-5.

[70] CMS 3000 Current Sensors, Sensitec Gmbh, Brochure, 2015, [Online], Available: https://www.sensitec.com/fileadmin/sensitec/Service_and_Support/Downloads/Product_Information/Brochures/SENSITEC_CMS3000_EN.pdf

[71] CMS 3100 Highly Dynamic MagnetoResistive Current Current Sensors, Sensitec Gmbh, Brochure, 2015, [Online], Available: https://www.sensitec.com/fileadmin/sensitec/Service_and_Support/Downloads/Data_Sheets/CMS3000/SENSITEC_CMS3100_DSE_01.pdf

[72] G. Laimer and J. W. Kolar, "Design and experimental analysis of a DC to 1 MHz closed loop magnetoresistive current sensor," Twentieth Annual IEEE Applied Power Electronics Conference and Exposition, 2005. APEC 2005, Austin, TX, 2005, pp. 1288-1292 Vol. 2.

[73] R. Slatter, "High accuracy, high bandwidth magnetoresistive current sensors for spacecraft power electronics," 2015 17th European Conference on Power Electronics and Applications (EPE'15 ECCE-Europe), Geneva, 2015, pp. 1-10.

[74] S. Scherner and R. Slatter, "New applications in power electronics for highly integrated high-speed magnetoresistive current sensors," 2013 15th European Conference on Power Electronics and Applications (EPE), Lille, 2013, pp. 1-10.

[75] S. Scherner and R. Slatter, "New applications in power electronics for highly integrated high-speed magnetoresistive current sensors," CIPS 2014; 8th International Conference on Integrated Power Electronics Systems, Nuremberg, Germany, 2014, pp. 1-7.

[76] J. Lenz and S. Edelstein, "Magnetic sensors and their applications," in IEEE Sensors Journal, vol. 6, no. 3, pp. 631-649, June 2006.

[77] AA and AB Series Analog Sensors, NVE Corp., Datasheet, 2017, [Online], Available: https://www.nve.com/analogSensors.php

[78] Application Notes for GMR Sensors, NVE Corp., Datasheet, 2017, [Online], Available: http://www.nve.com/Downloads/apps.pdf

[79] F. Xie, R. Weiss and R. Weigel, "Hysteresis Compensation Based on Controlled Current Pulses for Magnetoresistive Sensors," in IEEE Transactions on Industrial Electronics, vol. 62, no. 12, pp. 7804-7809, Dec. 2015.

[80] F. Xie, R. Weiss and R. Weigel, "Hysteresis Compensation Method for Magnetoresistive Sensors Based on Single Polar Controlled Magnetic Field Pulses," in IEEE Transactions on Industrial Electronics, vol. 64, no. 1, pp. 710-716, Jan. 2017.

[81] I. Jedlicska, R. Weiss and R. Weigel, "Linearizing the Output Characteristic of GMR Current Sensors Through Hysteresis Modeling," in IEEE Transactions on Industrial Electronics, vol. 57, no. 5, pp. 1728-1734, May 2010.

[82] J. Han, J. Hu, Y. Ouyang, S. X. Wang and J. He, "Hysteretic Modeling of Output Characteristics of Giant Magnetoresistive Current Sensors," in IEEE Transactions on Industrial Electronics, vol. 62, no. 1, pp. 516-524, Jan. 2015.

[83] I. Jedlicska, R. Weiss and R. Weigel, "Improving GMR current sensor measurements through hysteresis modeling," 2008 IEEE Power Electronics Specialists Conference, Rhodes, 2008, pp. 4781-4785.

[84] W. Kim, “Integrated Current Sensor using Giant Magneto Resistive (GMR) Field Detector for Planar Power Module,” MS Thesis, Virginia Polytechnic Institute and State University , Nov. 2012.

[85] W. Kim, S. Luo, G. Q. Lu and K. D. T. Ngo, "Integrated current sensor using giant magneto resistive (GMR) field detector for planar power module," 2013

Twenty-Eighth Annual IEEE Applied Power Electronics Conference and Exposition (APEC), Long Beach, CA, 2013, pp. 2498-2505.

[86] T. J. Brauhn, M. Sheng, B. A. Dow, H. Nogawa and R. D. Lorenz, "Module-integrated GMR-based current sensing for closed loop control of a motor drive," 2015 IEEE Energy Conversion Congress and Exposition (ECCE), Montreal, QC, 2015, pp. 342-349.

[87] P. E. Schneider, M. Horio and R. D. Lorenz, "Integrating GMR Field Detectors for High-Bandwidth Current Sensing in Power Electronic Modules," in IEEE Transactions on Industry Applications, vol. 48, no. 4, pp. 1432-1439, July-Aug. 2012.

[88] E. R. Olson and R. D. Lorenz, "Integrating giant magnetoresistive current and thermal sensors in power electronic modules," Applied Power Electronics Conference and Exposition, 2003. APEC '03. Eighteenth Annual IEEE, Miami Beach, FL, USA, 2003, pp. 773-777 vol.2.

[89] P. E. Schneider, M. Horio and R. D. Lorenz, "Integrating giant magneto-resistive (GMR) field detectors for high bandwidth current sensing in power electronic modules," 2010 IEEE Energy Conversion Congress and Exposition, Atlanta, GA, 2010, pp. 1260-1267.

[90] E. R. Oslon and R. D. Lorenz, "Integrated current sensing for power electronic modules using GMR field detectors," 2005 European Conference on Power Electronics and Applications, Dresden, 2005, pp. 9 pp.-P.9.

[91] P. E. Schneider, M. Horio and R. D. Lorenz, "Evaluation of Point Field Sensing in IGBT Modules for High-Bandwidth Current Measurement," in IEEE Transactions on Industry Applications, vol. 49, no. 3, pp. 1430-1437, May-June 2013.

[92] P. E. Schneider and R. D. Lorenz, "Evaluation of point field sensing in IGBT modules for high bandwidth current measurement," 2011 IEEE Energy Conversion Congress and Exposition, Phoenix, AZ, 2011, pp. 1950-1957.

[93] R. P. Singh and A. M. Khambadkone, "Giant Magneto Resistive (GMR) Effect Based Current Sensing Technique for Low Voltage/High Current Voltage Regulator Modules," in IEEE Transactions on Power Electronics, vol. 23, no. 2, pp. 915-925, March 2008.

[94] R. P. Singh and A. M. Khambadkone, "Giant Magneto Resistive (GMR) effect based Current Sensing Technique for DC/DC Converters," IECON 2007 - 33rd Annual Conference of the IEEE Industrial Electronics Society, Taipei, 2007, pp. 1420-1425.

[95] F. Xie, R. Weiss and R. Weigel, "Giant-Magnetoresistance-Based Galvanically Isolated Voltage and Current Measurements," in IEEE Transactions on Instrumentation and Measurement, vol. 64, no. 8, pp. 2048-2054, Aug. 2015.

[96] E. R. Olson and R. D. Lorenz, "Effective Use of Miniature Multipoint Field-Based Current Sensors Without Magnetic Cores," in IEEE Transactions on Industry Applications, vol. 46, no. 2, pp. 901-909, March-april 2010.

[97] Y. Ouyang, J. He, J. Hu, and S. X. Wang, “A current sensor based on the giant magnetoresistance effect: Design and potential smart grid applications,” Sensors, vol. 12, no. 11, pp. 15 520–15 541, Nov. 2012.

[98] N. Karrer and P. Hofer-Noser, "A new current measuring principle for power electronic applications," Power Semiconductor Devices and ICs, 1999. ISPSD '99. Proceedings., The 11th International Symposium on, Toronto, Ont., 1999, pp. 279-282.

[99] N. Karrer, P. Hofer-Noser and D. Henrard, "HOKA: a new isolated current measuring principle and its features," Conference Record of the 1999 IEEE Industry Applications Conference. Thirty-Forth IAS Annual Meeting (Cat. No.99CH36370), Phoenix, AZ, 1999, pp. 2121-2128 vol.3.

[100] L. Dalessandro, N. Karrer, M. Ciappa, A. Castellazzi and W. Fichtner, "Online and offline isolated current monitoring of parallel switched high-voltage multi-chip IGBT modules," 2008 IEEE Power Electronics Specialists Conference, Rhodes, 2008, pp. 2600-2606.

[101] G. Laimer and J. W. Kolar, "Wide bandwidth low complexity isolated current sensor to be employed in a 10 kW/500 kHz three-phase unity power factor PWM rectifier system," 2002 IEEE 33rd Annual IEEE Power Electronics Specialists Conference. Proceedings (Cat. No.02CH37289), 2002, pp. 1065-1070 vol.3.

[102] L. Dalessandro, N. Karrer and J. W. Kolar, "High-Performance Planar Isolated Current Sensor for Power Electronics Applications," in IEEE Transactions on Power Electronics, vol. 22, no. 5, pp. 1682-1692, Sept. 2007.

[103] L. Dalessandro, N. Karrer and J. W. Kolar, "A novel isolated current sensor for high-performance power electronics applications," Twenty-First Annual IEEE Applied Power Electronics Conference and Exposition, 2006. APEC '06., Dallas, TX, 2006, pp. 8 pp.-.

[104] J. Jiang and K. A. A. Makinwa, "Multipath Wide-Bandwidth CMOS Magnetic Sensors," in IEEE Journal of Solid-State Circuits, vol. 52, no. 1, pp. 198-209, Jan. 2017.

[105] J. Jiang and K. Makinwa, "11.3 A hybrid multipath CMOS magnetic sensor with 210??Trms resolution and 3MHz bandwidth for contactless current sensing," 2016 IEEE International Solid-State Circuits Conference (ISSCC), San Francisco, CA, 2016, pp. 204-205.

[106] S. J. Nibir, M. Biglarbegian and B. Parkhideh, "Performance study of magnetic field concentration techniques on magnetoresistor/rogowski contactless current sensor," 2016 IEEE SENSORS, Orlando, FL, 2016, pp. 1-3.

[107] B. Parkhideh; S. J. Nibir, "Hybrid Magnetoresistor-Planar Rogowski Current Sensing Scheme with Folded Trace Magnetic Field Concentration Technique," in IEEE Sensors Journal , vol.PP, no.99, pp.1-1.

[108] H. Jafarian et al., "Design and implementation of distributed control architecture of an AC-stacked PV inverter," 2015 IEEE Energy Conversion Congress and Exposition (ECCE), Montreal, QC, 2015, pp. 1130-1135.

[109] H. Jafarian, B. Parkhideh and S. Bhowmik, "A novel comparative robustness index for evaluating the performance of grid-tied PV inverters," 2016 IEEE 43rd Photovoltaic Specialists Conference (PVSC), Portland, OR, 2016, pp. 1254-1259.

[110] I. Mazhari, H. Jafarian, B. Parkhideh, S. Trivedi and S. Bhowmik, "Locking frequency band detection method for grid-tied PV inverter islanding protection," 2015 IEEE Energy Conversion Congress and Exposition (ECCE), Montreal, QC, 2015, pp. 1976-1981.

[111] H. Jafarian, B. Parkhideh, J. Enslin, R. Cox and S. Bhowmik, "On reactive power injection control of distributed grid-tied AC-stacked PV inverter architecture," 2016 IEEE Energy Conversion Congress and Exposition (ECCE), Milwaukee, WI, 2016, pp. 1-6.

[112] H. Jafarian, B. Parkhideh and S. Bhowmik, "Robustness evaluation of grid-tied AC-stacked PV inverter system considering manufacturing inaccuracies," IECON 2016 - 42nd Annual Conference of the IEEE Industrial Electronics Society, Florence, 2016, pp. 2378-2383.

[113] R. Perrin, N. Quentin, B. Allard, C. Martin, and M. Ali, “High temperature GaN active-clamp flyback converter with resonant operation mode,” IEEE J. of Emerg. And Selected Topics in Power Electro., Vol. 4, No. 3, September 2016.

[114] Y. Zhang, M. Rodriguez, and D. Maksimovic, “Very high frequency PWM buck converters using monolithic GaN half-bridge power stages with integrated gate drivers,” IEEE Trans. on Power Electro, Vol. 31, No. 11, November 2016.

[115] X. Huang, F. C. Lee, Q. Li, and W. Du, “High-frequency high-efficiency GaN-based interleaved CRM bidirectional Buck/Boost converter with inverse coupled inductor,” IEEE Trans. on Power Elctro, Vol. 31, No. 6, June 2016.

[116] D. Reusch, J. Strydom, and A. Lidow, “Thermal evaluation of chip-scale packaged Gallium Nitride transistors,” IEEE J. of Emerg. And Selected Topics in Power Electro., Vol. 4, No. 3, September 2016.

[117] L. Hoffmann, C. Gautier, S. Lefebvre, and F. Costa, “Optimization of the driver of GaN power transistor through measurement of their thermal behavior,” IEEE Trans. on Power Elctro, Vol. 29, No. 5, May 2014.